

Are Dry Mergers Dry, Moist, or Wet?

P. Sánchez-Blázquez^{1,2*}, B. K. Gibson¹, D. Kawata³, N. Cardiel⁴, and M. Balcells²

¹*Jeremiah Horrocks Institute for Astrophysics & Supercomputing, University of Central Lancashire, Preston, PR1 2HE, UK*

²*Instituto de Astrofísica de Canarias, c/Vía Lactea s/n, 38205, La Laguna, Tenerife, Spain*

³*Mullard Space Science Laboratory, Holmbury St. Mary, RH5 6NT, UK*

⁴*Departamento de Astrofísica y CC de la Atmósfera, Universidad Complutense de Madrid, Av Complutense s/n, 28040, Madrid, Spain*

Accepted

ABSTRACT

We present a spectral analysis of a sample of red-sequence galaxies identified by van Dokkum (2005) as dry merger remnants and ongoing dry mergers. Kinematics, stellar population absorption features, and ionisation from emission lines, are derived. We find that approximately half of the sample showing strong tidal features have younger stellar populations than a control sample at a given velocity dispersion. Conversely, galaxies with weak tidal tails and/or ongoing mergers – with the exception of one galaxy – do not show this young component. This seems to indicate that the young stellar populations observed in a significant fraction of ellipticals is the consequence of star formation triggered by mergers. This young component is consistent with a light “frosting” of young stars (<2% by mass) superimposed upon a dominant, old (~11 Gyr), stellar population. In terms of stellar populations, these mergers are, in fact, fairly dry. We found, however, that merger remnants with young stellar populations are supported by rotation, contrary to the expectations of a major dry merger. This suggests that the small amount of gas involved has been sufficient to produce a dynamically cold stellar component. Half of the galaxies with strong tidal distortion, however, are slow rotating and have stellar populations compatible with the control sample at a given velocity dispersion. Remarkably, none of the galaxies with velocity dispersions in excess of 250 km s⁻¹ have a young stellar component, independent of the merger stage.

Key words: Galaxies – galaxies: abundances – galaxies: elliptical and lenticular, cD – galaxies: evolution – galaxies: formation – galaxies: interactions – galaxies: kinematics and dynamics

1 INTRODUCTION

An accurate understanding of the physics underlying the formation and evolution of massive early-type galaxies remains a challenge. Within the Λ -dominated Cold Dark Matter hierarchical assembly framework, such galaxies are predicted to form over time through the progressive mergers of smaller galaxies (White & Frenk 1991; Cole et al. 2000), with the most massive systems assembling at relatively late epochs ($z \lesssim 1$). Such a scenario appears to be supported by several studies (Faber et al. 2007; Bell et al. 2006) that find an increase in the mass density function of the so-called “red-sequence” by factor of ~ 2 since $z \sim 1$.¹ Counter to this thought, the various tight scaling relations adhered to by elliptical galaxies (e.g. Fundamental Plane - Djorgovski & Davis 1987; the colour-magnitude and Mg- σ relationships - Bender, Burstein & Faber 1993; Kuntschner 2000) argues for a very early and coordinated formation of their stars.

This apparent contradiction can be resolved by separating the epoch of mass assembly from that of star formation, by assuming that the final mergers that lead to massive early-type galaxies are between gas-free progenitors – so-called “dry mergers”. Dry mergers and their implication for the formation of early-type galaxies have, for good reason, received an inordinate degree of recent attention (e.g. Bell et al. 2004; Tran et al. 2005; Khochfar & Burkert 2005; González-García & van Albada 2005; Faber et al. 2007; Naab, Khochfar & Burkert 2006; Bell et al. 2006; Boylan-Kolchin et al. 2006).

van Dokkum (2005; vD05, hereafter) analysed extremely deep images of red galaxies at redshifts $z \sim 0.1$ in the NOAO Deep Wide-Field Survey (Jannuzi & Dey 1999) and MUSYC (Gawiser et al. 2006) Survey and found that, amongst the bulge-dominated galaxies, 71% show tidal features over a scale of ~ 50 kpc. Because those features are red and diffuse, he concluded that, most likely, they are the consequence of interactions without associated star formation – i.e., dry mergers. vD05 also found that $\sim 50\%$ of the systems undergoing ongoing interactions have luminosity ratios $< 1:4$ – i.e., they are major mergers. He concluded that if the observed galaxies in ongoing mergers are representative of the progenitor’s remnants,

* E-mail: psanchez-blazquez@uclan.ac.uk

¹ Although this might not be strictly true for the *most* massive galaxies (Cimatti, Daddi & Renzini 2006; Ferreras et al. 2009)

then $\sim 35\%$ of the bulge-dominated galaxies have experienced a major dry merger in the recent past, underlying the importance of this mechanism in the evolution of early-type galaxies. vD05 further suggests that the observed increase in the stellar mass density of the red sequence since $z \sim 1$ could be the exclusive consequence of this process. However, this claimed relative importance has been questioned (Scarlata et al. 2007; Brown et al. 2008; Donovan, Hibbard & van Gorkom 2007).

Donovan et al. (2007) examined the possibility that “wet” (gas-rich) ellipticals might be identified as “dry” by the vD05 criteria. They found several examples of galaxies matching the dry merger criteria that contained significant amounts of neutral hydrogen ($\gtrsim 10^8 M_\odot$), as well as a significant degree of star formation in some cases. This possibility was reinforced by the work by Feldmann et al. (2008), where it was claimed that only a merger involving a dynamically cold disk could produce several of the observed tidal tail morphologies in the vD05 sample (specifically, the arm- and loop-like tails found in 60% of the major and 80% of the minor red-red galaxy mergers in the sample). In Kawata et al. (2006), we showed, using cosmological simulations, that red, diffuse tails similar to those seen by vD05 could be the consequence of minor mergers. Furthermore, numerical simulations have shown the difficulty in reproducing the anisotropy and ellipticity distribution of massive early-type galaxies with major dry mergers (e.g. Cox et al. 2006; Burkert et al. 2008), while conversely, several minor dry mergers appear to do a much better job in this regard.

If these mergers are gas-free and/or if the merger remnants are the consequence of minor instead of major mergers, the dry mergers might not be the only, or even the dominant, mechanism producing the observed evolution in the mass density of the red sequence as proposed by vD05. Furthermore, if the mergers are not entirely gas-free, and a small amount of star formation accompanied the interaction, the (nearly)-dry mergers might also explain the presence of the trace population of young stars seen in a large fraction of early-type galaxies and, therefore, the dispersion in the “mean” ages observed in several studies (González 1993; Trager et al. 2000; Caldwell et al. 2003; Sánchez-Blázquez et al. 2006).

If mergers are indeed central to the process of early-type galaxy formation, then the nature of the progenitors and the characteristics of the encounter become essential in describing the evolution of these systems. There is not yet a systematic study of the nature of the progenitors and of the merger remnant galaxies. Tran et al. (2005) performed spectroscopy of nine merging galaxy pairs identified by van Dokkum et al. (1999) in the cluster MS1054-03 at $z=0.83$, confirming that at least six were bound systems. They did not, however, perform a detailed analysis of the stellar content of these galaxies, due to the insufficient signal-to-noise ratio of the spectra (although they did show that the 4000\AA break was strong, characteristic of a population dominated by old G- and K-stars).

In what follows, we present a spectroscopic analysis of a sample of galaxies extracted from the vD05 catalogue, in order to analyse their stellar populations, the nature of any emission lines, and their kinematical properties. The questions that we wish to address are: (1) *Do the merger remnants contain a trace population of young stars?* A large number of elliptical galaxies contain such a trace population (e.g. Trager et al. 2000; Thomas et al. 2005; Caldwell et al. 2003; Sánchez-Blázquez et al. 2006b). The origin of this young population remains unclear – mergers, stars formed from gas re-accreted in a galactic cooling flow (Mathews & Brighenti 1999; Trager et al. 2000) or from satellite accretion, or star formation from gas released to the interstellar medium by old stars (Faber & Gallagher 1976; Ciotti et al. 1991) are but a few of the

proposed possibilities. (2) *Are these merger remnants rotationally supported?* It has been claimed that bright early-type galaxies supported by velocity anisotropies are the result of dry-mergers while rotationally-supported ellipticals are the result of mergers with gas (e.g. Cox et al. 2006, and references therein). By determining the degree of rotational support in these systems, we can confront this suggestion directly.

Section 2 describes the observations and data reduction, Section 3 the analysis of our spectra, including the determination of kinematical parameters and the measurement of line-strength indices, and Section 4 the results of this analysis. Section 5 summarises our conclusions.

2 OBSERVATIONS AND DATA REDUCTION

The galaxies analysed here are a subset of the ones presented in vD05. This sample was selected from the Multiwavelength Survey by Yale-Chile (MUSYC; Gawiser et al. 2006), and NOAO Deep Wide-Field Survey (NDWFS; Jannuzi & Dey 1999). Galaxies with magnitudes $R < 17$, and colours $1.6 \leq (B-R) \leq 2.2$ and with $(B-R) > 1.6 + 0.12 \times (R-15)$, were included in our analysis. This corresponds, roughly, to red, early-type galaxies with luminosities $L > L^*$ at redshifts $0.05 \lesssim z \lesssim 0.2$. Galaxies which were likely members of known clusters were also removed from the sample. We only observed those galaxies morphologically classified as bulge-dominated ellipticals or lenticulars.

vD05 found that half of the sample selected in this manner contains low surface brightness features indicative of interactions, such as plumes and tails. In the original sample of vD05, consisting in 126 galaxies, 44 (35%) show clear signs of past interactions and in an additional 23 cases (18%) the interaction is still in progress. Only 59 galaxies (47%) appear undisturbed, showing no unambiguous tidal features at the surface brightness limit of the survey. In his catalogue, vD05 flags those galaxies as “strong”, “weak”, “none”, or “ongoing”, depending upon the strength of the tidal features, and in the case of “ongoing”, indicating an ongoing interaction with another galaxy². In the “strong” category are the highly deformed merger remnants, whereas the “weak” class indicates more subtle features. vD05 suggests that the red ongoing mergers and the tidal features are very likely the consequence of the same physical process seen at different times. Galaxies with strong tidal features are seen shortly after the merger event and galaxies with weak features are observed at later times.

We selected, from the original sample, a sub-sample of galaxies comprising those catalogued as “ongoing”, “strong”, “weak”, and also “none” (unperturbed), the latter being used as a control sample. Table 1 summarises the main properties of the sample. Because we wanted to compare galaxies with similar properties in different stages of the merger, we tried to select galaxies with similar luminosity in the R-band, concentrating on the the brightest of the vD05 sample. Figure 1 shows a colour-magnitude diagram with the original sample from vD05. Overplotted are the galaxies selected for this study.

² Note that vD05 did not classify all the galaxy pairs as ongoing mergers but only those showing some morphological signs of interactions, such as tidal bridges, double nuclei in a common envelope, or tidal tails or fans with disturbed isophotes.

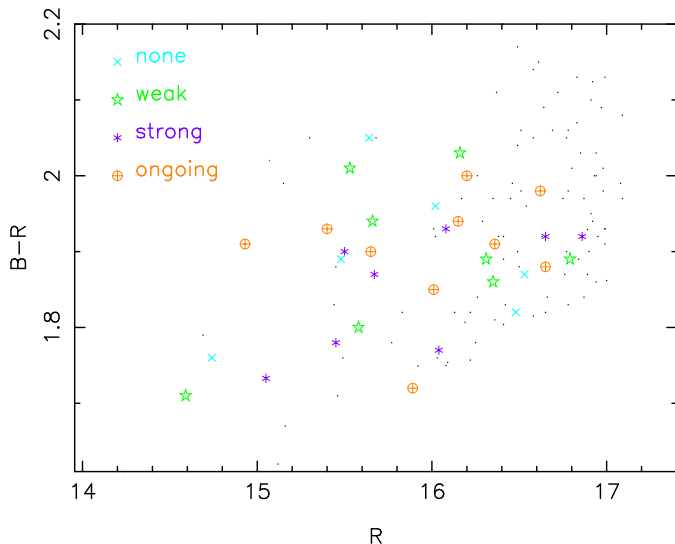


Figure 1. Colour-magnitude diagram of the 126 galaxies observed by vD05. We have marked, with different colors, the galaxies selected for this study. Of those, we have separated, with different symbols, galaxies in different merger stages, as indicated in the inset.

Long-slit spectroscopy was obtained along the major axis^{3,4} using the ISIS double spectrograph mounted at the f/11 Cassegrain focus on the William Herschel Telescope at the Roque de los Muchachos Observatory (La Palma, Spain) on two different runs, May 19-20 2006 and May 28-June 1 2008. We made use of the R600B grating with a 2-arcsec slit and the EEV12 detector, which provides a resolution $\text{FWHM}=4\text{\AA}$ ($\sigma = 102 \text{ km s}^{-1}$) in the unvignetted spectral range 3700-5260 \AA . In the red arm, we used the R600R grating with the MARCONI2 detector in the range 8100-9320 \AA . With our slit width, this provides us with a spectral resolution of $\text{FWHM}=3.6\text{\AA}$. We only present the data from the blue arm here, as the analysis of the Calcium Triplet will be the subject of a future paper. Typical exposure times for each galaxy were ~ 2 hours, although this varied depending upon the weather conditions.

Short exposures of 40 template stars from the MILES (Sánchez-Blázquez et al. 2006) stellar library were obtained to ensure that our data were in the same spectrophotometric system of that of the models employed during the analysis. Flat-field images were obtained at each position of the telescope to remove fringing in the red arm and to trace the relative response curve of the dichroic that depends upon the position of the telescope.

2.1 Data Reduction

The standard data reduction procedures (flat-fielding, cosmic ray removal, wavelength calibration, sky subtraction, and flux calibration) were performed with REDUCE (Cardiel 1999). This reduction package allows a parallel treatment of data and error frames and, therefore, produces an associated error spectrum for each individual data spectrum. Initial reduction of the CCD frames involved

bias and dark current subtraction, the removal of pixel-to-pixel sensitivity variations (using flat-field exposures of a tungsten calibration lamp), and correction for two dimensional low-frequency scale sensitivity variations (using twilight sky exposures). The dichroics in the ISIS spectrograph produce an intermediate frequency pattern (see Sánchez-Blázquez et al. 2006) which varies with the position of the telescope. As we were aware of this pre-existing problem from our earlier work, we acquired flat field images for every position of the telescope. Using these images, the fringing pattern was eliminated during the flat-fielding. Prior to the wavelength calibration, arc frames were used to correct the C-distortion in the images. This rotation correction guarantees alignment errors to be below 0.1 pixel. Spectra were converted to a linear wavelength scale using typically ~ 100 arc lines, fitted by third-order polynomials. The Root-Mean-Square (RMS) errors of the fits were $\sim 0.1 \text{\AA}$. All spectra were also corrected for S-distortion. Atmospheric extinction was calculated using the extinction curve provided by the Observatory. To correct for the effect of interstellar extinction, we used the curve of Fitzpatrick (1999). Foreground reddenings were obtained using the dust maps by Schlegel, Finkbeiner & Davis (1998). We used the IDL subroutines provided by the authors to read the maps and extract and $E(B-V)$ for each galaxy depending upon their Galactic coordinates. We corrected the continuum shapes of our spectra using exposures of 8-10 (depending on the run) standard stars. The final response curve was obtained as the average of all the individual curves while the difference between curves was used to derive an error in the indices due to flux calibration.

We extracted central spectra within an aperture of one effective radius (r_{eff}). Effective radii were calculated by fitting the two-dimensional spatial profile with a Sérsic law –as explained in Sec. 3.2 – the values for which are listed in Table 1. To study the rotational support of these galaxies, we also extracted spectra along the radius of each galaxy. We binned in the spatial direction to obtain a minimum signal-to-noise ratio per \AA of 20 in the region of $H\beta$.

3 MEASUREMENTS

3.1 Kinematics, velocity dispersion, and emission line removal

Velocity dispersions and radial velocities for the galaxies were measured using the IDL routine PPF (Cappellari & Emsellem 2004). This routine applies a maximum penalised likelihood formalism to extract as much information as possible from the spectra while suppressing the noise in the solution.

Surveys of large samples of bulge-dominated galaxies have revealed that 50-60% of these galaxies show weak optical emission lines (Caldwell 1984; Phillips et al. 1986; Goudfrooij et al. 1994). The measurement of several Lick/IDS indices can be affected by the presence of these lines. The effect on the Balmer lines is to lower the value of the index and, therefore, increase the derived mean age. To obtain emission line amplitudes and to separate the relative contribution of the stellar continuum from nebular emission in the spectra, we combine the PPF routine with GANDALF (Sarzi et al. 2006). This latter algorithm fits simultaneously the emission line kinematics using the optimal template convolved with the broadening function derived from PPF. One of the critical steps for the accurate measure of both emission lines and velocity dispersions is the calculation of a good template that reproduces the observed spectra. To build these templates we use a library of

³ The position angle was obtained by fitting ellipses to the images as described in Section 3.2

⁴ In the ongoing mergers where the two galaxies met the criteria to belong to the vD05 sample (2-3070/2-3102; 17-681/17-596; 19-2206/19-2242), the slit was oriented to pass through the two galaxies.

galaxy	Flag	redshift	r_{eff} ($''$)	r_{eff} kpc	n	b/a	v_{max} kms $^{-1}$	σ kms $^{-1}$
1-1403	none	0.132	4.6±0.8	10.9±1.9	4.07±0.53	0.68±0.02	20±14	292.6±5.5
11-1014	none	0.099	2.2±0.1	4.1±0.2	2.18±0.48	0.96±0.03	50±13	251.1±5.5
17-2031	none	0.099	1.7±0.4	3.2±0.7	2.13±2.36	0.62±0.05	60±17	188.1±7.7
18-2684	none	0.084	2.7±0.2	4.3±0.3	3.14±0.32	0.78±0.01	25±11	252.5±4.3
2-5013	none	0.133	2.8±0.1	6.5±0.2	2.40±0.80	0.90±0.02	60±9	139.1±7.3
22-991	none	0.085	2.4±0.3	3.7±0.5	5.22±1.80	0.70±0.01	25±26	175.6±4.5
10-232	weak	0.126	1.5±1.2	3.4±2.7	2.18±0.42	0.90±0.05	0±10	119.8±10.0
12-1734	weak	0.116	1.6±0.6	3.3±1.2	2.06±0.59	0.80±0.04	30±32	166.2±4.7
16-650	weak	0.128	3.4±0.1	7.7±0.2	2.05±0.60	0.66±0.04	10±17	197.2±6.9
22-790	weak	0.085	3.3±0.2	5.3±0.3	2.39±0.33	0.42±0.05	100±12	207.3±5.4
6-1553	weak	0.028	2.6±0.4	1.5±0.7	2.37±0.80	0.74±0.04	140±15	148.0±1.7
6-1676	weak	0.099	2.0±0.1	3.7±0.2	3.35±0.53	0.92±0.02	73±9	147.0±3.9
7-2322	weak	0.130	5.2±1.1	11.9±2.5	4.09±1.01	0.82±0.04	25±11	278.3±8.8
9-2105	weak	0.084	2.1±0.1	3.3±0.1	2.56±0.88	0.95±0.02	40±19	199.0±18.6
10-112	strong	0.128	2.3±0.6	5.2±1.3	1.95±2.50	0.69±0.07	160±16	164.4±6.6
1256-5723	strong	0.099	—	—	—	76±18	—	226.2±6.0
13-3813	strong	0.085	2.9±0.3	4.6±0.5	5.55±0.35	0.92±0.04	25±20	209.5±5.2
16-1302	strong	0.084	3.1±0.3	5.0±0.5	4.04±1.78	0.94±0.05	60±20	235.0±4.6
17-2134	strong	0.084	3.3±0.7	5.2±1.1	2.43±0.05	0.61±0.03	45±9	179.1±6.7
8-2119	strong	0.133	3.2±0.4	7.7±0.9	1.17±0.16	0.99±0.51	140±20	178.2±8.2
3-601	strong	0.153	2.5±0.8	6.6±2.1	2.73±0.90	0.60±0.02	60±9	195.3±5.5
5-994	strong	0.077	3.6±0.1	5.3±0.1	2.36±0.70	0.83±0.02	0±30	158.6±5.5
9-3079	strong	0.129	36.9±60.0	85.1±138	6.46±4.0	0.50±0.03	45±80	279.3±13.0
1-2874	ongoing	0.133	3.1±1.9	7.4±4.5	3.57±1.32	0.89±0.09	—	216.8±5.8
11-1278	ongoing	0.078	2.1±0.1	3.0±0.1	1.85±1.19	0.68±0.04	90±21	74.4±33.4
11-1732	ongoing	0.122	3.1±0.9	6.9±2.0	2.80±0.68	0.70±0.04	35±30	237.6±4.4
14-1401	ongoing	0.099	2.1±0.1	3.9±0.2	2.82±0.29	0.98±0.09	—	198.8±8.9
17-596	ongoing	0.084	32.5±40.7	51.4±64.3	6.87±2.13	0.79±0.05	90±20	215.5±5.8
17-681	ongoing	0.082	3.1±0.1	4.8±0.1	2.96±0.13	0.68±0.04	0±12	202.3±6.0
19-2242	ongoing	0.121	2.3±0.5	5.1±1.1	2.69±0.67	0.77±0.09	25±25	233.5±3.2
19-2206	ongoing	0.121	2.5±0.1	5.5±2.1	2.32±0.16	0.84±0.03	45±15	154.0±3.8
2-3070	ongoing	0.102	2.4±0.1	4.5±0.2	2.15±0.19	0.81±0.01	25±11	191.6±8.5
2-3102	ongoing	0.100	1.5±0.4	2.7±0.7	1.28±0.24	0.67±0.04	70±40	192.1±15.7

Table 1. Main characteristics of the sample: Col. 1: galaxy name; Col. 2: flag describing the type of tidal features in the galaxy, from vD05: *strong*: strong tidal features (these galaxies are generally highly-deformed merger remnants), *weak*: indicates more subtle features, such as tidal tails or shells, *ongoing*: ongoing interaction (both the primary and secondary galaxy show clear distortions or tidal tails); *none*: undisturbed galaxy; Col. 3: measured redshift; Col. 4: effective radius in arcsec; Col. 5: effective radius in kpc; Col. 6: Sérsic index; Col. 7: Ratio between minor and mayor axis calculated with GALFIT; Col. 8: maximum rotational velocity (calculated only in those cases where a regular rotation curve is observed – see appendix B); Col. 9: velocity dispersion measured within one effective radius;

stellar population models by Vazdekis et al. (2009, in preparation) based on the MILES stellar library (Sánchez-Blázquez et al. 2006; Cenarro et al. 2007). We include models with a wide range of ages (from 0.5 to 17 Gyr) and metallicities ($[Z/H]=-1.68$ to $+0.2$).

To estimate errors in the measured parameters, we perform Monte Carlo simulations repeating the measurement process for spectra perturbed with Gaussian noise, the latter for which is derived from the REDD_{fit}^{UGC} error spectra. Fifty simulations were performed and, each time, a new optimal template was calculated.

The rotation curves are shown in Appendix B. A maximum rotational velocity (v_{max}) was derived from these curves as half the difference between the peaks on the rotation curve. An error estimation of this value was done using the derived error bars for the velocity values and the difference between the maximum rotational velocity measured at the two sides from the centre of the galaxy. Some of the galaxies do not show regular rotation curves. In particular U-shaped curves, as predicted in merger simulations (Combes et al. 1995) are observed in some of the ongoing merg-

ers. In those cases, a v_{max} was not derived. The v_{max} values and the velocity dispersion inside r_{eff} are shown in Table 1.

3.2 Structural parameters

We used the code GALFIT (Peng et al. 2002) to estimate structural parameters, i.e., ellipticities (ϵ), effective radius (r_{eff}) and Sérsic indices, using the publicly-available images from the Third Data Release of the NOAO Deep Wide-Field Survey. The images were obtained with the KPNO Mayall 4m telescope and MOSAIC-1 imager. We use the images in the Bw-band (the Bw filter has a bluer central wavelength than the standard Johnson B-band filter). GALFIT convolves Sérsic (1968) $r^{1/n}$ galaxy models with the PSF of the images, and determines the best fit by comparing the convolved model with the galaxy surface brightness distribution using a Levenberg-Marquardt algorithm to minimise the χ^2 of the fit. The PSF has been obtained from isolated stars, as close as possible to the observed galaxies. The Sérsic index n measures the shape of the

surface brightness profiles, where $n=1$ represent an exponential and $n=4$ a de Vaucouleurs profile. During the fit, neighbouring galaxies were excluded using a mask, but in the case of closely neighbouring objects or interacting galaxies, both objects were fitted simultaneously. The measured parameters with this process are listed in Table 1. We have tested the internal consistency of our data, comparing the size and shape of our galaxies in different bands, i.e., Bw, R and I. The seeing and depth of those images are slightly different, which allows us to test the robustness of our derived parameters. Of course, this test is only valid under the assumption that the change in size and shape of the light profile of the galaxies due to changes in the wavelength along the given filters is smaller than the intrinsic error in estimating the structural parameters. Fig. 2 shows the comparison between the sizes, Sérsic indices and ellipticities calculated in the different bands. We estimate the error in the parameters as the mean difference between the parameters in the different bands.

3.3 Line-strength indices

We measure Lick/IDS line-strength indices as defined by Trager et al. (1998) with the additional definitions by Worthey & Ottaviani (1997) for the higher-order Balmer lines $H\delta$ and $H\gamma$. Our wavelength range did not allow us to measure lines such as Mgb, Fe5270, and Fe5335 for most of the galaxies. In particular, we were not able to measure any feature with high sensitivity to Mg variations, which limits our ability to obtain an accurate estimates of both $[Mg/Fe]$ and the ages. Errors in the indices were estimated from the uncertainties caused by photon noise, wavelength calibration, and flux calibration.

Lick/IDS indices depend on the broadening of the spectra due to the blending of lines in the pass-band definition. In order to compare the indices of different galaxies with each other these have to be corrected to the same level of intrinsic Doppler and instrumental broadenings. When comparing with stellar population models based on the Lick/IDS system (Vazdekis 1999; Worthey 1994; Thomas et al. 2003) one must follow two steps: (1) degrade the spectra to the wavelength-dependent instrumental resolution of this library, and (2) make a correction due to the velocity dispersion of the galaxy. The broadening correction depends on the strength of the indices and is difficult to apply accurately. In most cases, it does introduce systematic effects in the final measurements which, in some cases, can dominate the final error (see, e.g., Kelson et al. 2006).

In this paper we do not use models based on the Lick system but the new models by Vazdekis et al. (2009). The latter reflect a significant improvement upon the earlier models of the Vazdekis et al. (2003), due to the use of the new MILES stellar library (Sánchez-Blázquez et al. 2006) and its associated extended coverage in stellar atmospheric parameter-space. As the library is fully flux-calibrated the models not only predict spectral features, but the entire spectrum from 3500 to 7500Å. The use of these models allows us to choose the resolution at which we want to measure our indices. After careful consideration, we decided to measure all our indices in spectra with a total broadening of 300 km s^{-1} . All the spectra were broadened by σ_{broad} , such that $300 = \sqrt{\sigma_{\text{gal}}^2 + \sigma_{\text{ins}}^2 + \sigma_{\text{broad}}^2}$, where σ_{gal} is the velocity dispersion of the galaxy and σ_{ins} the instrumental resolution in km s^{-1} . By doing so, we avoid any further correction due to the velocity dispersion of the galaxies and, therefore, avoid the introduction of systematic errors, as mentioned above.

Our sample contains galaxies with a range of redshifts, and so

Index	α	Type
$H\delta_A$	-0.721 ± 0.508	1
$H\delta_F$	-0.206 ± 0.249	1
CN ₂	0.059 ± 0.030	2
Ca4227	0.047 ± 0.075	1
G4300	0.027 ± 0.022	1
$H\gamma_A$	-0.850 ± 0.422	2
$H\gamma_F$	-0.436 ± 0.321	2
Fe4383	0.061 ± 0.033	1
Ca4455	0.097 ± 0.075	1
Fe4531	0.040 ± 0.021	1
C4668	0.119 ± 0.049	1
$H\beta$	-0.050 ± 0.190	1

Table 2. α coefficient and corresponding error for the aperture correction. The final column indicates whether the correction is additive (1) or multiplicative (2).

a fixed aperture samples different regions of each. Despite having added spectra within one r_{eff} for all the galaxies, we still have to make a correction due to aperture effects, as the width of the slit is fixed to 2 arcsec. To do this we have made use of the aperture corrections derived by Sánchez-Blázquez et al. (2009) obtained using a large sample of line-strength gradients from Sánchez-Blázquez et al. (2006c; 2007). The aperture correction of the atomic indices can be written as (Jørgensen 1995):

$$\log(I_{\text{reff}}) = \log(I_{\text{med}}) + \alpha \log \frac{r_{\text{med}}}{r_{\text{eff}}} \quad (1)$$

where $r_{\text{med}} = 1.025 \times \sqrt{\frac{2 \times r_{\text{eff}}}{\pi}}$, while that of the molecular indices and the higher-order Balmer lines can be written as:

$$(I_{\text{reff}}) = (I_{\text{med}}) + \alpha \log \frac{r_{\text{med}}}{r_{\text{eff}}} \quad (2)$$

This aperture correction is very uncertain, as elliptical galaxies show a large scatter in their gradients and there are no clear correlations between the line-strength gradients and other parameters of the galaxies. However, the aperture corrections for our galaxies are very small and none of our results change should the aperture correction not be applied. Table 2 shows the α coefficient for all the indices, while Table A1 in appendix 3.3 shows the fully-corrected indices at $\sim 300 \text{ km s}^{-1}$ resolution.

4 ANALYSIS

4.1 Nature of the emission lines

Active nuclei may play a role during mergers, preventing the gas from cooling and forming stars and, therefore, leaving the remnant red (Kawata et al. 2006; Springel, di Matteo & Hernquist 2005). It is therefore interesting to compare the degree of nuclear activity in the merger remnants with those of the undisturbed galaxies.

To examine the possible presence of nuclear activity in our sample, we adopt here the same criteria as in Sarzi et al. (2006) and consider that emission is present when the line protrudes above the noise in the stellar spectrum by more than a factor of four times for all the lines, except for $H\beta$, for which we lower this to three. Baldwin et al. (1981) proposed a suite of three diagnostic diagrams to classify the dominant energy source in emission line galaxies. These diagrams are based on the four optical line ratios $[OII]/H\beta$, $[NII]/H\alpha$, $[SII]/H\alpha$, and $[OI]/H\alpha$. We do not possess sufficient lines

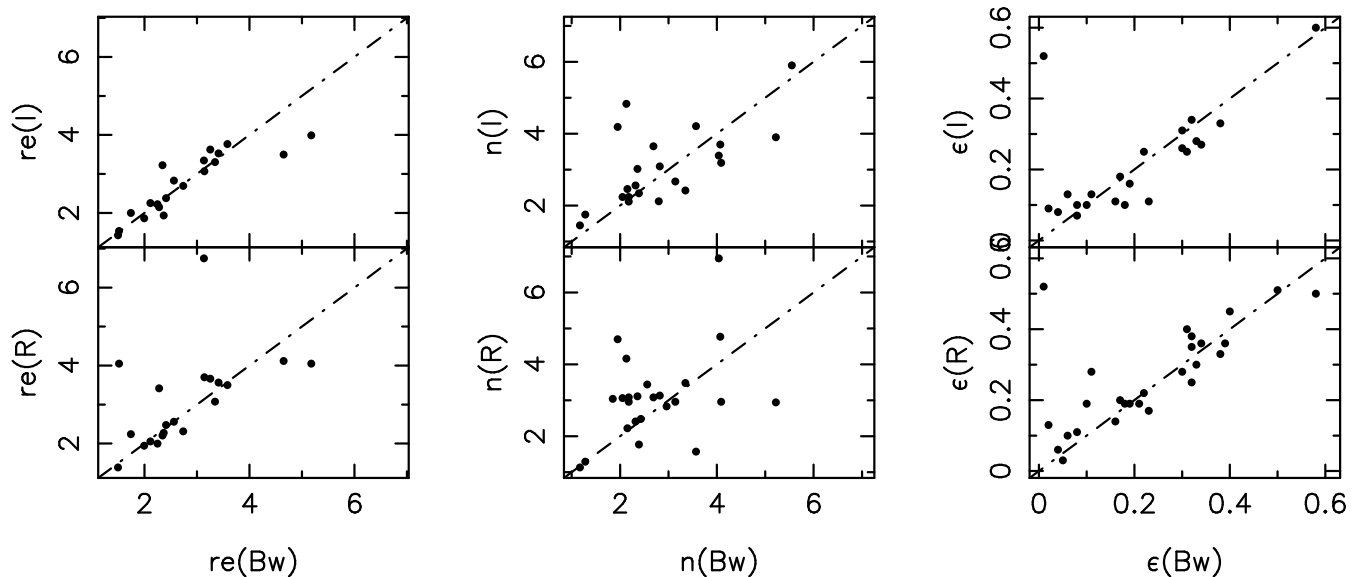


Figure 2. Comparison of the structural parameters derived in different band-passes.

in our wavelength range to plot our galaxies in several of the classical diagnostic diagrams. However, we can infer approximately the nature of ionisation in several of them. Yan et al. (2006) studied the source of ionisation in a sample of red-sequence galaxies from the Sloan Digital Sky Survey (SDSS). They showed that galaxies with high-values of $[\text{OII}]/\text{H}\alpha$ have relatively uniform line ratios in $[\text{OII}]/\text{H}\alpha$, $[\text{OIII}]/\text{H}\beta$, $[\text{NII}]/\text{H}\alpha$, $[\text{OI}]/\text{H}\alpha$, and $[\text{OIII}]/[\text{OII}]$, and were identifiable as LINER-type objects. Galaxies with lower values of $[\text{OIII}]/\text{H}\beta$ could be star forming galaxies, transition objects, or Seyferts. The wavelength range of our spectra does not allow us to measure $\text{H}\alpha$ so, instead, we use $\text{H}\beta$. Yan et al. (2006) calculate a median value of $\text{H}\alpha/\text{H}\beta=4.46$ before applying any reddening correction to their sample of red-sequence galaxies. The demarcation proposed by these authors to separate star forming galaxies from other categories is: $\text{EW}[\text{OII}] < 18 \text{EW}(\text{H}\beta) - 6$. To separate between LINERs and Seyferts we use the theoretical line derived by Kewley & Ellison (2008) based on the ratio $[\text{OIII}]/[\text{OII}]$, which is an indicator of the ionisation parameter of the gas. Roughly, Seyfert galaxies show ratios $[\text{OIII}]/[\text{OII}] > 1$, while lower ratios are characteristic of LINERs. Table 3 shows the equivalent widths of the different emission lines calculated for our sample of galaxies.

We see an enhanced occurrence of emission lines in merger remnants and ongoing mergers with respect to the sample of undisturbed galaxies, although the number of galaxies is small to make definitive conclusions.

It can be seen in Table 3 that most galaxies showing emission lines have line-ratios compatible with being LINERs or Seyferts. None of the spectra present line ratios consistent with ongoing star formation, although $\sim 35\%$ of the sample showing emission could not be accurately classified due to their insufficient detection. Our classifications would not be affected for smaller assumed values of $\text{H}\alpha/\text{H}\beta$, however if the ratio was significantly larger, perhaps due to the presence of dust, the incidence of star forming galaxies could be larger. We conclude that, under the limitations of our sample and assumptions, we do not detect an enhancement of *current* star formation line-ratios in galaxies now experiencing a merger (or with strong signs of recent interactions).

An example of a galaxy spectrum with LINER-type emission is shown in Figure 3. The origin of emission lines in LINERs, (low-

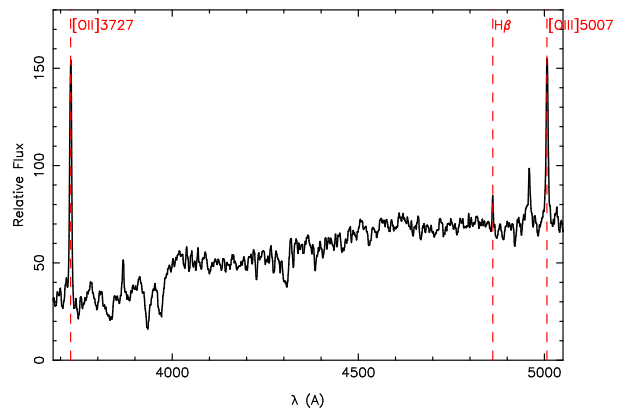


Figure 3. Spectra of 10-232, a galaxy with LINER-type emission.

ionisation narrow emission line regions – Heckman 1980) is still unknown. An AGN power source, fast shocks, photoionisation by hot stars, or photoionisation by an old metal-rich population, are several of the proposed possibilities (see Kewley et al. 2006 for a discussion). Most likely, the current definition of LINER encompasses more than one type of ionisation mechanism. However, in a sample of red galaxies extracted from SDSS, Graves et al. (2006) found that those with LINER-like emission were systematically 10-40% younger than their emission-free counterparts, suggesting a connection between the mechanism powering the emission (the possibilities being AGN, post-AGB stars, shocks, or cooling flows) and more recent star formation in the galaxies. The enhanced emission in merger remnants in our sample suggests that mergers might be the triggering mechanism for both star formation and emission, producing gravitational torques capable of driving radial flows towards the centre of the galaxies (Hernquist 1989; Barnes & Hernquist 1991).

4.2 Rotational support

Major dry and wet mergers, and minor mergers, can all produce red, bulge-dominated galaxies, but the kinematical structure of the

gal		EW[OII] (Å)	EW H β (Å)	EW([OIII]) (Å)	class
1-1403	none	No	No	No	No emission
11-1014	none	No	No	No	No emission
17-2031	none	No	No	No	No emission
18-2684	none	–	No	No	No emission
2-5013	none	7.9	No	No	LINER
22-991	none	No	No	No	No emission
10-232	weak	6.21	2.97	12.52	Seyfert
12-1734	weak	No	No	No	No emission
16-650	weak	0.58	–	–	?
22-790	weak	–	No	No	No emission
6-1553	weak	–	No	0.76	?
6-1676	weak	0.71	No	1.25	Seyfert
7-2322	weak	0.45	–	–	?
9-2105	weak	–	1.72	4.71	?
10-112	strong	0.47	No	No	LINER
1256-5723	strong	2.80	No	1.15	LINER
13-3813	strong	–	No	No	No emission
16-1302	strong	–	0.93	1.74	?
17-2134	strong	–	2.99	1.56	?
8-2119	strong	0.71	0.81	–	LINER/Seyfert
3-601	strong	0.70	–	–	?
5-994	strong	–	No	0.65	?
9-3079	strong	No	No	No	No emission
1-2874	ongoing	No	No	No	No emission
11-1278	ongoing	–	No	1.37	?
11-1732	ongoing	3.5	0.77	0.85	LINER
14-1401	ongoing	0.80	No	1.2	Seyfert
17-596	ongoing	–	No	No	No emission
17-681	ongoing	–	No	No	No emission
19-2242	ongoing	No	No	No	No emission
19-2206	ongoing	0.39	No	No	LINER
2-3070	ongoing	2.37	0.81	1.49	LINER
2-3102	ongoing	1.69	No	1.33	LINER

Table 3. Emission line detection in our sample of galaxies; First and second column give the name of the galaxy and the characteristics of the morphological perturbations. Columns 3, 4, and 5 indicate the detection (or not) of emission in [OII] $\lambda\lambda$ 3727, H β , and [OIII] $\lambda\lambda$ 5007. We consider a detection when the line protrudes more than a factor of three above the noise.

remnant is expected to be very different (Cox et al. 2006; Bornaud, Jog & Combes 2005; Naab & Burkert 2003). Observations indicate that most luminous galaxies show box-shaped isophotes and little rotation, while less luminous spheroids show disk-shaped isophotes and exhibit rotation along the photometric major axis (Davies et al. 1983; Bender et al. 1989; Faber et al. 1997; Kormendy & Bender 1996). Major dry mergers cannot produce rotating remnants (Cox et al. 2006, although see González-García & Balcells 2005 for a different point of view), while minor mergers or mergers with a gaseous component can both produce rotationally supported bulge dominated galaxies (Naab & Burkert 2003; Cox et al. 2006).

Figure 4 shows the relation between v_{\max} and σ (v/σ in the plot) against ellipticity, the so-called anisotropy diagram. This diagram quantifies the relative contribution of ordered and random motions to the overall kinematics of each galaxy. The solid line indicates the expected relationship for an oblate spheroid with an isotropic velocity distribution. Recently, the SAURON collaboration have shown that the anisotropy diagram is not entirely adequate to describe the kinematic structure of spheroidal galaxies (Emsellem et al. 2007; Cappellari et al. 2007). They define a new quantity, λ_R , that is linked to the baryonic angular momentum. Us-

ing this parameter, they separate the galaxies into slow- ($\lambda_R < 0.1$) and fast-rotators ($\lambda_R > 0.1$). 2D spectroscopy is necessary to measure the λ_R parameter, but Cappellari et al. (2007) show that fast- and slow-rotators occupy different regions of the anisotropy diagram. To compare with this study, we have plotted in Figure 4, the slow- and fast-rotators from the SAURON database (Emsellem et al. 2007).

As can be seen, our sample shows different degrees of rotational support. Two out of eight galaxies with strong signs of recent interactions – for which we could measure ellipticities – are in the same zone of the diagram as the SAURON fast rotators. Two others deviate from the region populated by early-type galaxies towards much higher rotational velocities while another two occupy the same regions as the slow-rotators from the SAURON sample. The rest of the galaxies in this sub-sample (two) lie in the transition region between slow- and fast-rotators. Clearly, the nature of the merger remnants is not unique, reflecting, most likely, the different nature of the progenitors. Half of the “weak” and “undisturbed” galaxies, and half of the systems in “ongoing” mergers, are also compatible with being supported by rotation

Among ellipticals, those with higher σ tend to be supported

by velocity anisotropies while those with small σ tend to be supported by rotation (Bender et al. 1998). Therefore, the percentage of rotationally-supported galaxies might depend on the σ of each sub-sample. To explore if this is the case, we have also plotted in Fig. 4 the relation between (v/σ) and σ . It can be seen that, in agreement with the SAURON sample, low-rotators span a wide range of σ and there are no fast rotators galaxies with $\sigma > 250 \text{ km s}^{-1}$. The distribution of galaxies in the v/σ diagram is very similar to that of the SAURON galaxies, independent of the morphological disturbances of the sample. The only exceptions are three merger remnants (two in the “strong” group and one in the “weak”) showing a very high value of v/σ . The very high (v/σ) values can be explained if there is a decrease in the central σ due to the formation of a cold disc (so-called σ -drops). The standard explanation for these drops is the presence of cold central stellar discs originating from gas inflow (Emsellem et al. 2001; Wozniak et al. 2003). Wozniak & Champavert (2006) predict that these features last until the fresh gas ceases flowing into the centre to form stars. Therefore, these are not long-lived. A scenario where these features get formed during the merger process, when there is enough gas, but do not last very long, could explain why they do not appear in the SAURON sample.

To summarize, with the exception of three galaxies with very high v/σ , the distribution of merger remnants in the anisotropy diagram is not different to that of a sample of normal early-type galaxies. We do not find that *all* of our remnants are supported by velocity anisotropies, as would be expected if they were all remnants of major dry mergers (Cox et al. 2006), but some of them are.

Figure 5 shows the relation between the Sérsic index and the central velocity dispersion for our sample of galaxies. As can be seen, we also do not find any difference between the distribution of Sérsic indices for the galaxies in different merger stages and the control sample.

4.3 Index- σ relations

Elliptical galaxies show tight correlations between line-strength indices and the central velocity dispersions; Figure 6 show this relation for our sample. We also show a linear fit to the sample of undisturbed galaxies. As can be appreciated, 4 of the 9 galaxies with strong morphological signs of recent merger activity show systematically weaker metallic lines and stronger Balmer lines at a given velocity dispersion than those undisturbed or with only weak signs of recent interactions. One of the galaxies in an ongoing merger, 11-1732, also shows these strong deviations from the fit defined by the undisturbed galaxies.

4.4 Comparison with SSPs

The deviations from the index- σ relations observed for half of the merger remnants with strong signs of recent interactions – i.e., weaker metal-lines and stronger Balmer lines than the undisturbed galaxies – can be the consequence of a younger population, a more metal-poor population, or a combination of both. This is due to the age-metallicity degeneracy that affects the line-strength indices, as well as broad-band colors (Worthey 1994). However, some (Balmer) lines are more sensitive to age variations than to metallicity variations and, therefore, by combining them with a non-Balmer line, one can partially break the degeneracy between these two parameters. Figure 7 shows several index-index diagrams combining different metal-indices with Balmer lines. Overplotted are the

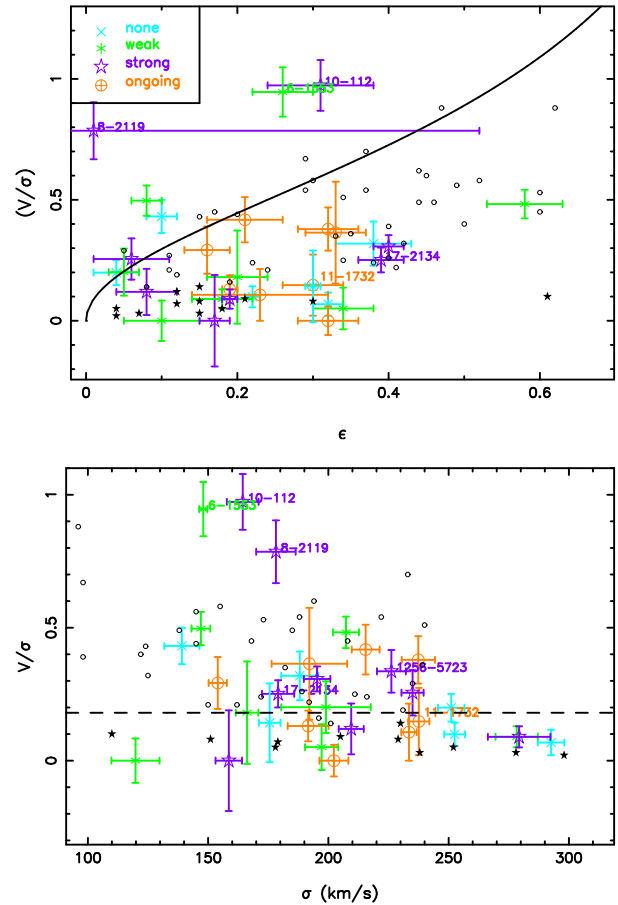


Figure 4. Top Panel: $(V_{\max}/\sigma, \epsilon)$ diagram for our sample. Small open circles and filled stars correspond to the fast- and slow-rotators from the SAURON database, respectively. The line corresponds to the relation expected for an isotropic, oblate, edge-on rotators, in the revised formalism for integral field kinematics of Binney (2005). Lower panel: $(V_{\max}/\sigma, \sigma)$ diagram for our sample. The dashed line show the approximate demarcation between slow- and fast-rotators.

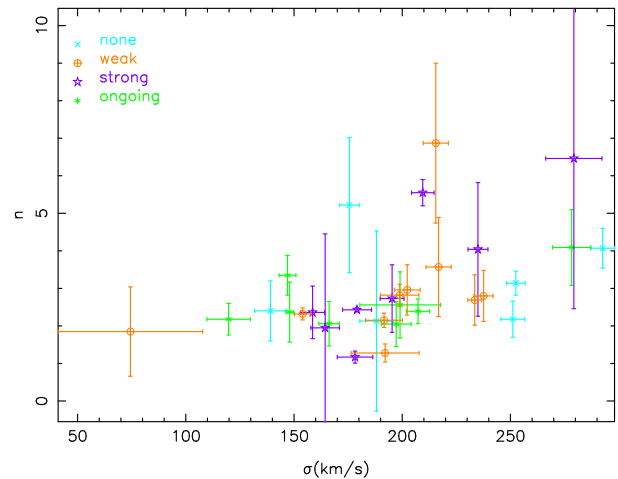


Figure 5. Relation between the Sérsic index (n) and the central velocity dispersion for our sample of galaxies.

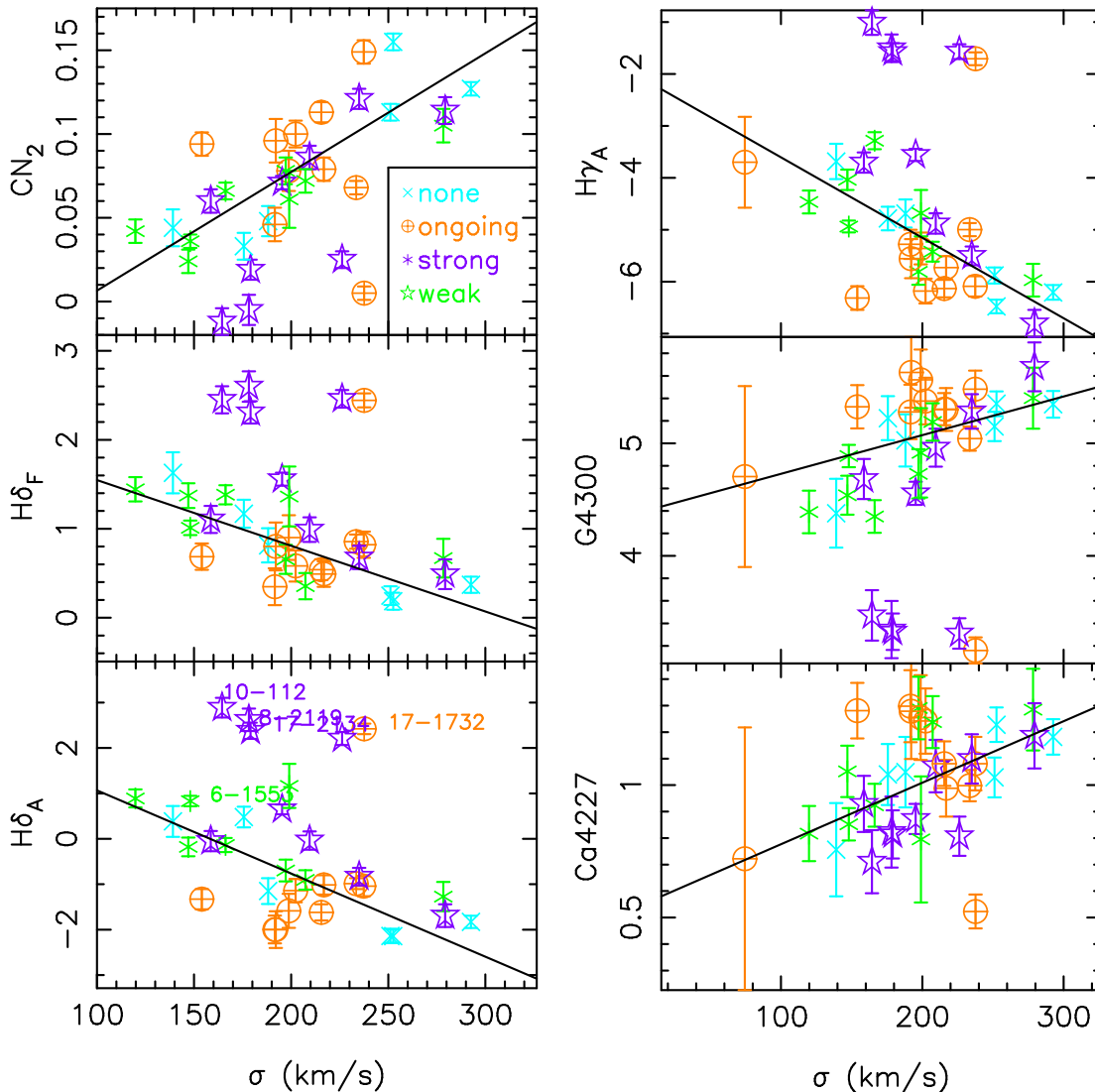


Figure 6. Relation between line-strength indices and velocity dispersion measured in an aperture of one effective radius. Galaxies with no or weak signs of recent interactions are represented with blue and green crosses, respectively; galaxies with strong signatures of recent interactions are plotted with purple stars, while ongoing mergers are represented in orange. A linear fit to the galaxies without any signs of recent interactions (labeled as “none”) is also shown.

single-stellar population (SSP) models of Vazdekis et al. (2009) for populations of different ages (horizontal lines) and metallicities (vertical lines), as indicated in the labels.

It can be seen from those figures that \sim half of the galaxies with strong signs of recent interactions are, indeed, younger⁵ than those undisturbed or with weak signs of recent interactions. However, they are as metal-rich as the other galaxies.

This behaviour indicates that at least some of the “red” mergers were not completely dry. 11-1732, a galaxy in an ongoing merger, also shows a young component, indicating that, most likely, in this merger some star formation has been triggered. All the galaxies with a mean younger population show LINER-type emission lines.

⁵ When we use the term “younger” (or more metal-rich), we mean they they have a lower single-stellar population (SSP)-equivalent age (higher SSP-equivalent metallicity). As we show later in the paper, this does not mean that the galaxy as a whole is younger, because even a small contaminating population of young stars can bias this age towards low values.

From these index-index diagrams, ages and metallicity could be derived. The primary drawback to deriving an accurate age from the integrated light of a single-age single-abundance stellar population is the complication of abundance ratio effects, i.e., the fact that the ratio between different chemical elements is not always the same in the systems under study as in the solar neighbourhood (Worthey 1998). In particular, giant elliptical galaxies show enhanced levels of α -elements with respect to Fe. Several authors have developed methods to correct for these effects, and significant progress has been made (Tantalo et al. 1998; Trager et al. 2000a; Thomas et al. 2003; Cohelo et al. 2007; Dotter et al. 2007; Lee et al. 2008). However, in order to apply these methods, lines with sensitivities to different chemical element variations are needed. In our case, the derivation of accurate ages is compromised as our wavelength range did not allow us to measure any of the Mg-sensitive Lick-indices. In any case, none of the conclusions of this paper requires the derivation of accurate values of age and metallicity.

Furthermore, the ages and chemical abundances derived from these models are SSP-equivalent parameters, i.e., the stellar popula-

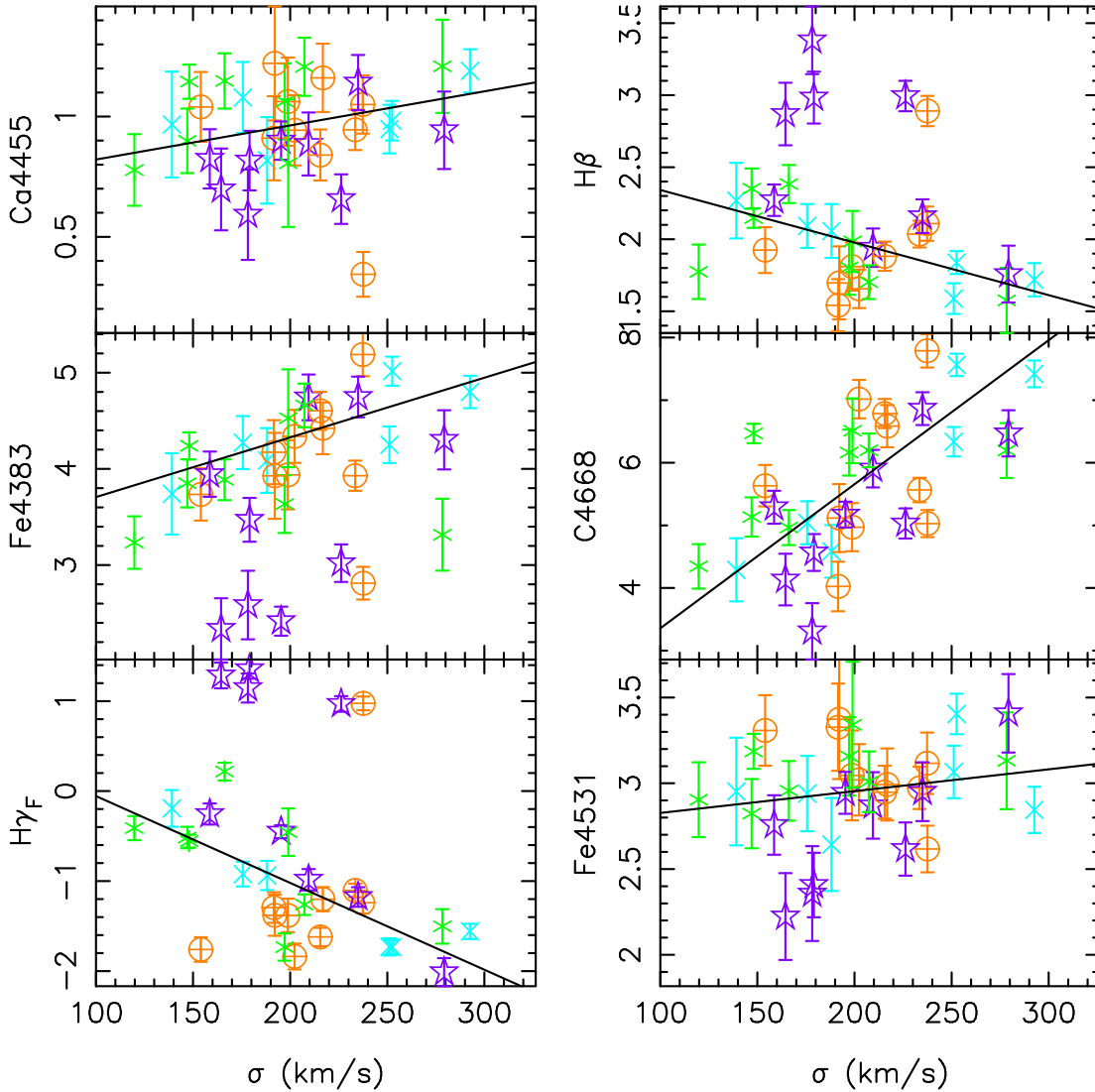


Figure 6. Continued

tion of the galaxies if all the stars were coeval and chemically homogeneous. We know that this is likely not the case for our objects. It is well-known that even very small amounts of recent star formation can bias the final mean ages derived with single-stellar populations (e.g., Trager et al. 2000b). The exact amount depends on the age of the burst. If the tidal tails are produced in a major merger event, those would last for only a few hundred Myrs (vD05), meaning that the young population would be quite young. A small fraction of these very young stars would change the measured indices dramatically. On the contrary, if the tidal tails have been produced in minor mergers, then they are believed to last longer ($\sim 1-2$ Gyr), and the fraction of new stars formed may be larger.

To quantify the degree of “pollution” from such new stars that could be present in our galaxies, we have added to an underlying population of age 11 Gyr (corresponding, roughly to a redshift formation of three in our cosmology), different bursts of young stars with ages from 0.1 to 1.3 Gyr. We have also varied the light-fraction of the burst from 1 to 30% in the V-band. This translates into different mass fractions of the burst, depending on the age of the young population.

Figure 8 shows the variation of the line-strength indices as a

function of the mass fraction of the burst. We built these diagrams using stellar population models by Vazdekis et al. (2009) with solar metallicity for both the underlying “old” and superimposed “new” burst populations. If we make the assumption that most of the stars in our sample are old and with metallicities around solar, and that the deviations from the index- σ relation defined by the unperturbed sample are due to a young component formed in the merger, we can calculate the amount of new stars as a function of the mass fraction of the young population and of its age.

In the figure, we have indicated, with horizontal lines, the deviations from the index- σ relation ($I_{gal} - I_{fit}$) for the galaxies with strong signs of recent interactions, that deviate more from the index- σ relations (8-2119, 1256-5723, 10-112 and 17-2134). These galaxies will give us an upper limit to the amount of young stars in our sample.

It can be seen that, if the young population is younger than 0.1 Gyr, the mass fraction has to be lower than 1% in order to reproduce the observed indices. If the tidal features have lasted for 1.5 Gyr, the observed variations in the indices from the index- σ relation are reproduced with mass fractions always lower than 2%. The masses of the sample of galaxies with strong signs of recent

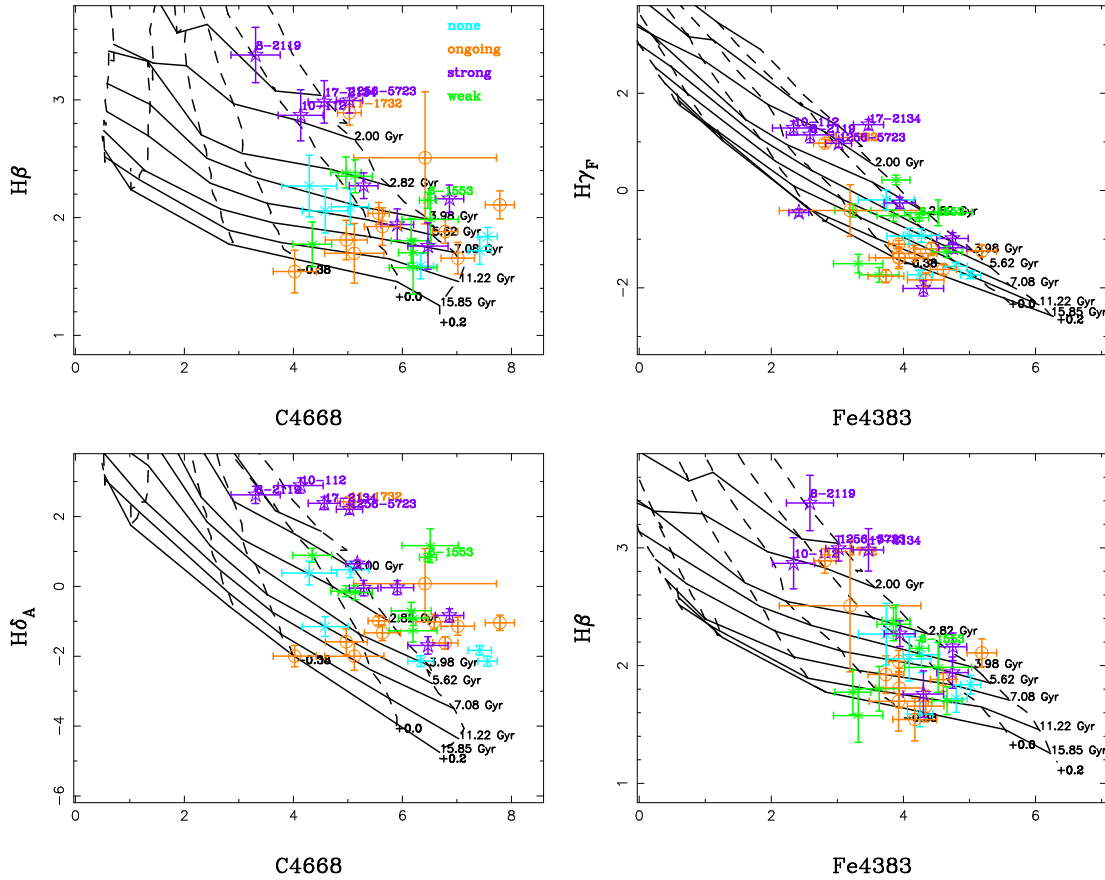


Figure 7. Index-index diagram combining a metal-sensitive index with a Balmer line, more sensitive to age variations. Overplotted are the models of Vazdekis et al. (2009) for different values of age and metallicity. Symbols are the same as in Figure 4. As can be seen, galaxies with strong signatures of having experienced a recent merger, plotted in purple, deviate systematically from the relation defined by the control sample. The deviation is toward strong Balmer lines and weaker metallic lines, which is expected in the presence of a young population.

interactions oscillate between $\sim 2 \times 10^{10}$ and $\sim 1.1 \times 10^{11} M_{\odot}$ – 1% of the total mass translates into a $\sim 10^8$ - $10^9 M_{\odot}$ burst of star formation. These numbers are compatible with the masses of gas found by Donovan et al. (2007) of 1 - $6 \times 10^8 M_{\odot}$ for their sample of red galaxies selected in a similar way as vD05. This amount of gas can come from a dwarf galaxy in a minor interaction (the total HI mass of a dwarf galaxy is on the order of 10^7 - $10^8 M_{\odot}$ (Gebel, Gallagher & Harbeck 2003) or from a gas poor system (such as a low-luminosity elliptical), with typical masses of a few times $10^8 M_{\odot}$ (Phillips et al. 1986).

This means that, in terms of new stars formed, these mergers are fairly dry. Only a small fraction of stars are formed. However, because these mergers appear to be very common (72% of the bulge-dominated red galaxies from vD05 sample show morphological disturbances), they offer a good explanation for the number of elliptical galaxies showing mean-young stellar populations.

5 DISCUSSION

In this paper we have characterised the properties of a sample of galaxies chosen to be remnants of dry mergers or red galaxies in the process of merging from the sub-sample of vD05. We have observed galaxies classified as having “weak” and “strong” morphological disturbances as well as galaxies in ongoing interactions. We

have compared their properties with an undisturbed control sample extracted from the same field.

We found a large variety in the properties of the galaxies with signs of having experienced recent interactions. Independently of the strength of the morphological distortions, our sample contains both, slow- and fast-rotators and galaxies with Sérsic indices varying between ~ 2 and 4. The only difference between our merger remnants and the control sample is that galaxies with strong signs of recent interactions show, more often, the presence of young stellar populations. However, the line-strength indices can be explained as a composition of an old population (~ 11 Gyr) and a trace component of young stars ($\lesssim 2\%$, by mass) if the stars are younger than 1-2 Gyr (which is the maximum time the morphological signatures are expected to survive). Given the stellar mass of our galaxies (between 2×10^{10} and $\sim 10^{11} M_{\odot}$), this translates into masses between 1 - $6 \times 10^8 M_{\odot}$. This agrees with recent results by Donovan et al. (2007) who found HI at the level of $10^8 M_{\odot}$ in a sample of galaxies selected to pass the same colour selection criteria as that in vD05. Whitaker & van Dokkum (2008) argued that the Donovan et al. (2007) sample was not representative of the red-merger population and that the gas-to-stellar mass ratio in the vD05 sample was, at least, two orders-of-magnitude lower than in the Donovan et al. sample ($M_{\text{gas}}/M_{\text{star}} < 3 \times 10^{-4}$). They also concluded that the gas content in the vD05 sample was independent of the tidal distortion parameter, “strong”, “weak”, or “none”. They were all, essentially, gas-free galaxies. Our results are in apparent contradiction to this

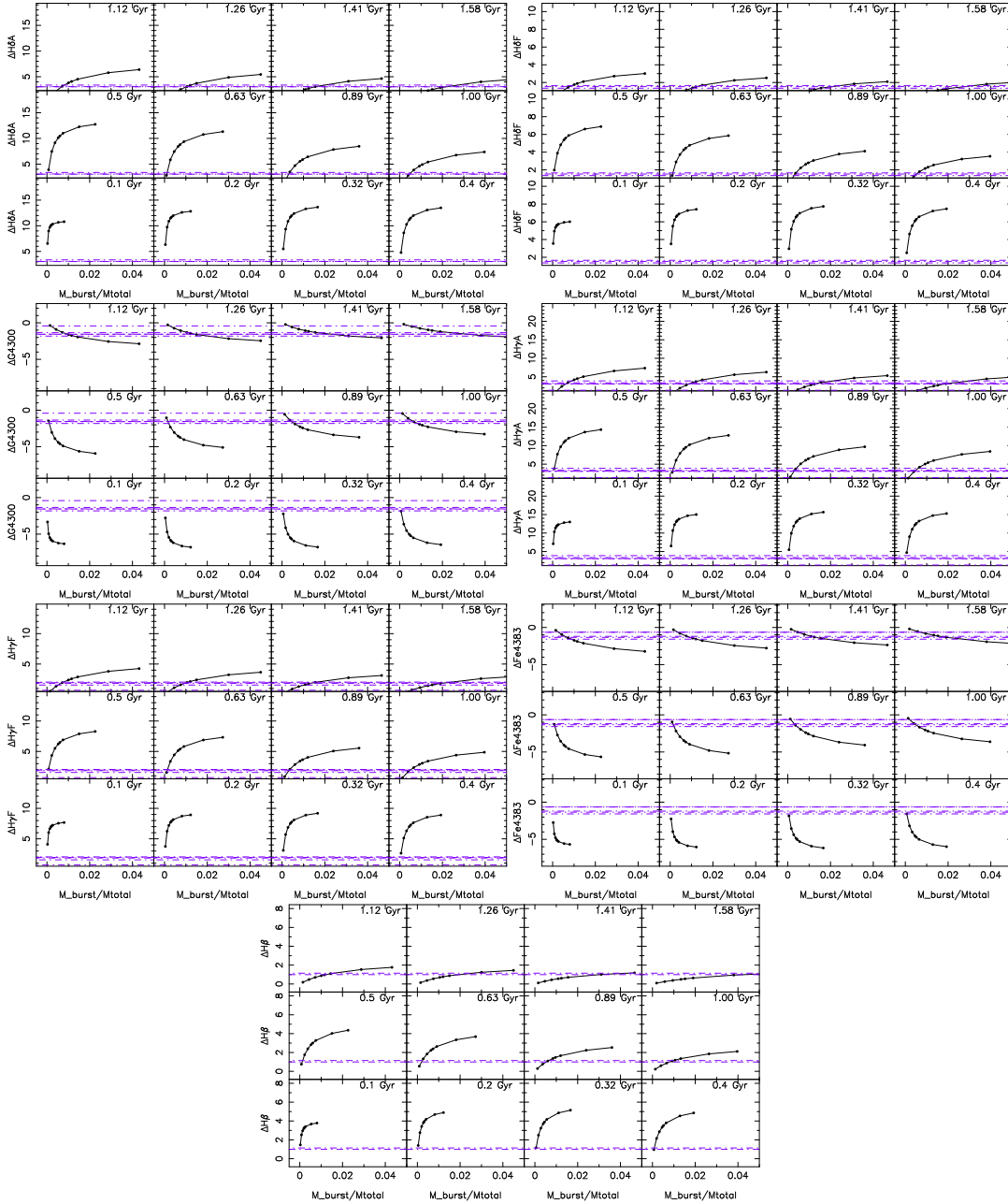


Figure 8. Variation of line-strength when adding to an underlying old population of age 11 Gyr and solar metallicity, a younger population of the age and mass fraction indicated in the insets . Purple lines represent the residuals with respect to the index- σ relation of the galaxies with strong signs of recent interactions. Only those values that are 3 times greater than the errors are shown.

conclusion, however it is difficult to assess the veracity of this discrepancy, as the Whitaker & van Dokkum derivation of the gas content was indirect, inferred via the appearance of dust in HST images and, as such, are likely to be lower limits to the true gas content.

If we assume that galaxies in ongoing mergers are representative of the progenitors of our merger remnants, we can study this issue in our ongoing sample. In our sample of ongoing mergers, we have three major merger systems⁶, 19-2242/19-2206; 17-596/17-681, and 2-3070/2-3102; the rest (four galaxies) are in ongoing minor mergers. Except in the case of 2-3079/2-3102, the other two

major mergers show clear tidal tails and loops, which are difficult to reproduce without the presence of a cold component in one of the galaxies. However, none of these galaxies show a young stellar component. (Mihos & Hernquist 1994) showed that in mergers between bulge-dominated galaxies, most of the star formation happens when the galaxies coalesce. This could explain the lack of young stars in these systems. Among the other four galaxies in minor mergers, the only galaxy with a clear young component is 11-1732. We do not find any systematic difference between the stellar populations of those galaxies involved in major and minor mergers. We note that most of the galaxies in ongoing interactions are systematically below the index-index relations in the Balmer lines and above in the metal lines. We speculate that this may be due to a

⁶ Defined as those with a luminosity ratio between the galaxies below 1:3

decrease in the central velocity dispersion in the first stages of the merger, although this would have to be modeled numerically.

Regarding the possible differences between galaxies with “strong” and “weak” morphological disturbances, vD05 proposed that the intensity of the disturbances in the final remnant was the consequence of an evolutionary sequence. In this way, galaxies with “weak” morphological disturbances would be the same objects as galaxies with “strong” ones in a later stage of the merger. On the other hand, Feldman et al. (2008) proposed, based on the morphology of the disturbances, that galaxies with “weak” perturbations could be the “true” remnants of major dry mergers (while those remnants with “strong” disturbances were more compatible with being wet). Our analysis of stellar populations supports both views; in the first case, if the mass fractions of the young populations are of the order of 1-2%, these would not be visible any longer after a short period of time (<1 Gyr). On the other hand, the stellar populations are also compatible with a truly dry merger, as they are almost indistinguishable from the control sample.

The scenario of the minor mergers can also be discussed for those galaxies with “strong” signs of recent interactions. vD05 argue that the progenitors of the remnants are typically major mergers rather than low accretion events, because low accretion events would produce much fainter debris, undetectable in the MUSYC and NOAO surveys. Also because the fraction of tidally disturbed galaxies that he found amongst disk-dominated galaxies was much lower than among bulge-dominated galaxies (only 8% of the disk dominated galaxies show tidal features as opposed to 62% of the bulge-dominated galaxies), he claims this is consistent with the idea that the events responsible for the tidal features are strong enough to destroy any dominant disk component. Furthermore, the features vD05 detected are red, suggesting that the progenitors had old stellar populations. However, Kawata et al. (2006) and Feldman et al. (2008) argue that the types of structures observed in the MUSYC and NOAO images can be explained by minor interactions. Our analysis of stellar populations suggests, however, that major mergers are more likely mechanism. This is because the metallicity of galaxies with young stellar populations is quite large. Dwarf galaxies have lower metal content than more massive ones (Skillman, Kennicutt & Hodge 1989; Tremonti et al. 2004). If the new stars formed from gas coming from a dwarf galaxy we would expect to measure, at least for a short period of time (~ 1 Gyr), a lower-mean metallicity in the integrated spectrum (Serra & Trager 2007), which is not observed. However, the sample of galaxies with young stellar components is small and this analysis need to be done in a larger sample to extract firmer conclusions.

It has been suggested that there is a transition mass above which red-galaxies formed, exclusively, via dry interactions (e.g., Faber et al. 2007). The break point is at $1-2 \times 10^{11} M_{\odot}$, or $M_B = -20$ to -21 , where boxy and disky ellipticals coexist (Faber et al. 2007; Lauer et al. 2007). This mass corresponds to $\sigma \sim 250$ km s $^{-1}$ (Faber & Jackson 1976). Despite the small number of galaxies in our sample with σ in excess of 250 km s $^{-1}$, we found that they are all slow-rotators and show old stellar populations. However, the scenario of major dry mergers to produce boxy, non-rotating, and very isotropic early-type galaxies, have been called into question in several works (Cox et al. 2006; Burkert et al. 2008). In particular, is difficult to reproduce the small anisotropies and ellipticities observed in massive elliptical galaxies in dissipationless simulations of mergers between two galaxies of similar mass. On the contrary, an accumulation of minor dry mergers can produce the observed remnants (Burkert et al. 2008). One possibility is that most of the interactions suffered by these galaxies are minor, but that the relative contribu-

tion of the young stars to the galaxy is lower in the most massive systems.

6 CONCLUSIONS

In this paper we have studied the properties of a sample of red merger remnants or red galaxies in the process of merging extracted from vD05. We have observed galaxies classified as having “weak” and “strong” morphological disturbances as well as galaxies in ongoing interactions. We have compared their properties with an undisturbed control sample extracted from the same field. Our main results can be summarized as follows:

- There is rich mixture in the properties of the galaxies with signs of having experience recent interactions. Independently of the strength of the morphological distortions, our sample contains both, slow- and fast-rotators and galaxies with Sérsic indices compatible with exponential and de Vaucouleurs profile.
- Galaxies with strong signs of recent interactions show, more often, the presence of young stellar populations, indicating that, despite the red colour of the remnant, the mergers were not *completely* dry.
- These young components, however, can be explained with a frosting $\sim 2\%$ in mass of young stars on the top of an old population. Therefore, the mergers are fairly dry in terms of stellar populations. However, these galaxies with young stellar components are all compatible with being supported by rotation. Therefore, the cold component is enough to produce a disc.
- We found a larger incidence of emission lines in our sample of strong merger remnants compared with the control sample. The emission line ratios are compatible with being LINER- and Seyfert-type. The origin of emission in LINER galaxies is not well-understood. Graves et al. (2006) found that red-galaxies with LINER-like emission were systematically 10-40% younger than their emission-free counterparts, suggesting a connection between the mechanism powering the emission and more recent star formation in the galaxies. Based on our small sample, we suggest that the mechanism triggering both is the fueling of gas towards the centre produced by the gravitational torques in galaxy mergers.
- The previous results can be summarise saying that the population of red merger remnants observed by vD05 is compatible with containing remnants of mergers with and without gas. For the formers, we favour major mergers as the metallicity of the young component seems to be very large.

ACKNOWLEDGMENTS

PSB acknowledges the support of a Marie Curie Intra-European Fellowship within the 6th European Community Framework Programme. BKG acknowledges the support of the UK’s Science & Technology Facilities Council (STFC Grant ST/F002432/1) and the Commonwealth Cosmology Initiative. This paper is based on observations obtained at the William Herschel Telescope, operated by the Isaac Newton Group in the Spanish Observatorio del Roque de los Muchachos of the Instituto de Astrofísica de Canarias. NC acknowledges financial support from the Spanish Programa Nacional de Astronomía y Astrofísica under grant AYA2006–15698–C02–02

REFERENCES

- Baldwin J. A., Phillips M. M., Terlevich R., 1981, *PASP*, 93, 5
- Bell E. F., Phleps S., Somerville R. S., Wolf C., Borch A., Meisenheimer K., 2006, *ApJ*, 652, 270
- Bell E. F., Wolf C., Meisenheimer K., Rix H.-W., Borch A., Dye S., Kleinheinrich M., Wisotzki L., McIntosh D. H., 2004, *ApJ*, 608, 752
- Bender R., Burstein D., Faber S. M., 1993, *ApJ*, 411, 153
- Bender R., Saglia R. P., Ziegler B., Belloni P., Greggio L., Hopp U., Bruzual G., 1998, *ApJ*, 493, 529
- Bender R., Surma P., Doebereiner S., Moellenhoff C., Madejsky R., 1989, *A&A*, 217, 35
- Binney J., 2005, *MNRAS*, 363, 937
- Bournaud F., Jog C. J., Combes F., 2005, *A&A*, 437, 69
- Boylan-Kolchin M., Ma C.-P., Quataert E., 2006, *MNRAS*, 369, 1081
- Brown M. J. I., Zheng Z., White M., Dey A., Jannuzi B. T., Benson A. J., Brand K., Brodwin M., Croton D. J., 2008, *ApJ*, 682, 937
- Burkert A., Naab T., Johansson P. H., Jesseit R., 2008, *ApJ*, 685, 897
- Caldwell N., 1984, *ApJ*, 278, 96
- Caldwell N., Rose J. A., Concannon K. D., 2003, *AJ*, 125, 2891
- Cappellari M., Emsellem E., Bacon R., Bureau M., Davies R. L., de Zeeuw P. T., Falcón-Barroso J., Krajnović D., Kuntschner H., McDermid R. M., Peletier R. F., Sarzi M., van den Bosch R. C. E., van de Ven G., 2007, *MNRAS*, 379, 418
- Cardiel N., 1999, PhD thesis, , Universidad Complutense de Madrid, Spain, (1999)
- Cenarro A. J., Peletier R. F., Sánchez-Blázquez P., Selam S. O., Toloba E., Cardiel N., Falcón-Barroso J., Gorgas J., Jiménez-Vicente J., Vazdekis A., 2007, *MNRAS*, 374, 664
- Cimatti A., Daddi E., Renzini A., 2006, *A&A*, 453, L29
- Ciotti L., D’Ercole A., Pellegrini S., Renzini A., 1991, *ApJ*, 376, 380
- Coelho P., Bruzual G., Charlot S., Weiss A., Barbuy B., Ferguson J. W., 2007, *MNRAS*, 382, 498
- Cole S., Lacey C. G., Baugh C. M., Frenk C. S., 2000, *MNRAS*, 319, 168
- Combes F., Rampazzo R., Bonfanti P. P., Pringniel P., Sulentic J. W., 1995, *A&A*, 297, 37
- Cox T. J., Dutta S. N., Di Matteo T., Hernquist L., Hopkins P. F., Robertson B., Springel V., 2006, *ApJ*, 650, 791
- Davies R. L., Efstathiou G., Fall S. M., Illingworth G., Schechter P. L., 1983, *ApJ*, 266, 41
- Djorgovski S., Davis M., 1987, *ApJ*, 313, 59
- Donovan J. L., Hibbard J. E., van Gorkom J. H., 2007, *AJ*, 134, 1118
- Dotter A., Chaboyer B., Ferguson J. W., Lee H.-c., Worthey G., Jevremović D., Baron E., 2007, *ApJ*, 666, 403
- Emsellem E., Cappellari M., Krajnović D., van de Ven G., Bacon R., Bureau M., Davies R. L., de Zeeuw P. T., Falcón-Barroso J., Kuntschner H., McDermid R., Peletier R. F., Sarzi M., 2007, *MNRAS*, 379, 401
- Emsellem E., Greusard D., Combes F., Friedli D., Leon S., Pécontal E., Wozniak H., 2001, *A&A*, 368, 52
- Faber S. M., Gallagher J. S., 1976, *ApJ*, 204, 365
- Faber S. M., Jackson R. E., 1976, *ApJ*, 204, 668
- Faber S. M., Tremaine S., Ajhar e. a., 1997, *AJ*, 114, 1771
- Faber S. M., Willmer C. N. A., Wolf C., Koo D. C., Weiner B. J., Newman J. A., et al. 2007, *ApJ*, 665, 265
- Feldmann R., Mayer L., Carollo C. M., 2008, *ApJ*, 684, 1062
- Ferreras I., Lisker T., Pasquali A., Khochfar S., Kaviraj S., 2009, ArXiv e-prints
- Fitzpatrick E. L., 1999, *PASP*, 111, 63
- Gawiser E., van Dokkum P. G., Herrera D., 2006, *ApJS*, 162, 1
- González J. J., 1993, Ph.D. Thesis
- González-García A. C., van Albada T. S., 2005, *MNRAS*, 361, 1043
- Goudfrooij P., Hansen L., Jorgensen H. E., Norgaard-Nielsen H. U., 1994, *A&AS*, 105, 341
- Graves G. J., Faber S. M., Schiavon R. P., Yan R., 2007, *ApJ*, 671, 243
- Grebel E. K., Gallagher III J. S., Harbeck D., 2003, *AJ*, 125, 1926
- Jannuzi B. T., Dey A., 1999, in Weymann R., Storrie-Lombardi L., Sawicki M., Brunner R., eds, *Photometric Redshifts and the Detection of High Redshift Galaxies Vol. 191 of Astronomical Society of the Pacific Conference Series, The NOAO Deep Wide-Field Survey*. pp 111+–
- Jorgensen I., Franx M., Kjaergaard P., 1995, *MNRAS*, 276, 1341
- Kawata D., Mulchaey J. S., Gibson B. K., Sánchez-Blázquez P., 2006, *ApJ*, 648, 969
- Kelson D. D., Illingworth G. D., Franx M., van Dokkum P. G., 2006, *ApJ*, 653, 159
- Kewley L. J., Ellison S. L., 2008, *ApJ*, 681, 1183
- Khochfar S., Burkert A., 2005, *MNRAS*, 359, 1379
- Kormendy J., Bender R., 1996, *ApJ*, 464, L119+
- Kuntschner H., 2000, *MNRAS*, 315, 184
- Lauer T. R., Gebhardt K., Faber S. M., Richstone D., Tremaine S., Kormendy J., Aller M. C., Bender R., Dressler A., Filippenko A. V., Green R., Ho L. C., 2007, *ApJ*, 664, 226
- Lee H. ., Worthey G., Dotter A., Chaboyer B., Jevremovic D., Baron E., Briley M. M., Ferguson J. W., Coelho P., Trager S. C., 2008, ArXiv e-prints
- Mathews W. G., Brighenti F., 1999, *ApJ*, 527, L31
- Mihos J. C., Hernquist L., 1994, *ApJ*, 431, L9
- Naab T., Burkert A., 2003, *ApJ*, 597, 893
- Naab T., Khochfar S., Burkert A., 2006, *ApJ*, 636, L81
- Phillips M. M., Jenkins C. R., Dopita M. A., Sadler E. M., Binette L., 1986, *AJ*, 91, 1062
- Sánchez-Blázquez P., Forbes D. A., Strader J., Brodie J., Proctor R., 2007, *MNRAS*, 377, 759
- Sánchez-Blázquez P., Gorgas J., Cardiel N., 2006, *A&A*, 457, 823
- Sánchez-Blázquez P., Gorgas J., Cardiel N., González J. J., 2006, *A&A*, 457, 787
- Sanchez-Blazquez P., Jablonka P., Noll S., Poggianti B. M., Moustakas J., Milvang-Jensen B., Halliday C., et al. 2009, ArXiv e-prints
- Sánchez-Blázquez P., Peletier R. F., Jiménez-Vicente J., Cardiel N., Cenarro A. J., Falcón-Barroso J., Gorgas J., Selam S., Vazdekis A., 2006, *MNRAS*, 371, 703
- Sarzi M., Falcón-Barroso J., Davies R. L., Bacon R., Bureau M., Cappellari M., de Zeeuw P. T., Emsellem E., Fathi K., Krajnović D., Kuntschner H., McDermid R. M., Peletier R. F., 2006, *MNRAS*, 366, 1151
- Scarlata C., Carollo C. M., Lilly S. J. e. a., 2007, *ApJS*, 172, 494
- Schlegel D. J., Finkbeiner D. P., Davis M., 1998, *ApJ*, 500, 525
- Serra P., Trager S. C., 2007, *MNRAS*, 374, 769
- Skillman E. D., Kennicutt R. C., Hodge P. W., 1989, *ApJ*, 347, 875
- Springel V., Di Matteo T., Hernquist L., 2005, *ApJ*, 620, L79
- Tantalo R., Chiosi C., Bressan A., 1998, *A&A*, 333, 419
- Thomas D., Maraston C., Bender R., 2003, *MNRAS*, 343, 279

- Thomas D., Maraston C., Bender R., Mendes de Oliveira C., 2005, *ApJ*, 621, 673
- Trager S. C., Faber S. M., Worthey G., González J. J., 2000a, *AJ*, 120, 165
- Trager S. C., Faber S. M., Worthey G., González J. J., 2000b, *AJ*, 120, 165
- Trager S. C., Faber S. M., Worthey G., González J. J., 2000c, *AJ*, 119, 1645
- Trager S. C., Worthey G., Faber S. M., Burstein D., Gonzalez J. J., 1998, *ApJS*, 116, 1
- Tran K.-V. H., van Dokkum P., Franx M., Illingworth G. D., Kelson D. D., Schreiber N. M. F., 2005, *ApJ*, 627, L25
- Tremonti C. A., Heckman T. M., Kauffmann G., Brinchmann J., Charlot S., White S. D. M., Seibert M., Peng E. W., Schlegel D. J., Uomoto A., Fukugita M., Brinkmann J., 2004, *ApJ*, 613, 898
- van Dokkum P. G., Franx M., Fabricant D., Kelson D. D., Illingworth G. D., 1999, *ApJ*, 520, L95
- Vazdekis A., 1999, *ApJ*, 513, 224
- Vazdekis A., Cenarro A. J., Gorgas J., Cardiel N., Peletier R. F., 2003, *MNRAS*, 340, 1317
- Whitaker K. E., van Dokkum P. G., 2008, *ApJ*, 676, L105
- White S. D. M., Frenk C. S., 1991, *ApJ*, 379, 52
- Worthey G., 1994, *ApJS*, 95, 107
- Worthey G., Ottaviani D. L., 1997, *ApJS*, 111, 377
- Wozniak H., Champavert N., 2006, *MNRAS*, 369, 853
- Wozniak H., Combes F., Emsellem E., Friedli D., 2003, *A&A*, 409, 469
- Yan R., Newman J. A., Faber S. M., Konidaris N., Koo D., Davis M., 2006, *ApJ*, 648, 281

APPENDIX A: LINE-STRENGTH INDICES

Table A1 shows the line-strength indices measured on the galaxy spectra.

APPENDIX B: ROTATION CURVES

Figure B1 shows the observed line-of-sight velocity as a function of the projected radius for the galaxies of our sample.

	CN ₁	CN ₂	Ca4227	G4300	Fe4383	Ca4455	Fe4531	C4668	H β	H δ_A	H δ_F	H γ_A	H γ_F
1-1403	0.089	0.127	1.182	5.347	4.799	1.190	2.845	7.419	1.719	-1.829	0.371	-6.206	-1.559
	0.004	0.004	0.067	0.118	0.168	0.090	0.135	0.213	0.115	0.136	0.091	0.142	0.085
11-1014	0.084	0.113	1.029	5.150	4.251	0.948	3.066	6.335	1.588	-2.139	0.249	-5.880	-1.731
	0.004	0.005	0.075	0.130	0.190	0.101	0.153	0.235	0.107	0.158	0.105	0.154	0.095
17-2031	0.024	0.048	1.049	5.026	4.087	0.818	2.643	4.584	2.057	-1.151	0.814	-4.687	-0.938
	0.008	0.009	0.133	0.232	0.336	0.180	0.271	0.419	0.187	0.284	0.192	0.269	0.163
18-2684	0.118	0.155	1.228	5.352	5.016	0.983	3.404	7.563	1.838	-2.143	0.186	-6.477	-1.734
	0.004	0.005	0.065	0.110	0.151	0.082	0.118	0.178	0.079	0.144	0.096	0.130	0.078
2-5013	0.011	0.044	0.756	4.379	4.113	0.967	2.952	4.723	1.760	0.383	1.629	-3.640	-0.192
	0.009	0.011	0.176	0.306	0.422	0.220	0.314	0.504	0.262	0.341	0.230	0.340	0.204
22-991	-0.012	0.033	1.040	5.224	4.273	1.079	2.940	5.042	2.092	0.479	1.170	-4.783	-0.922
	0.007	0.008	0.115	0.195	0.275	0.148	0.220	0.344	0.152	0.228	0.157	0.227	0.137
10-232	0.011	0.042	0.817	4.390	3.690	0.778	2.904	4.610	1.774	0.890	1.444	-4.496	-0.411
	0.006	0.007	0.104	0.189	0.273	0.149	0.218	0.356	0.189	0.198	0.136	0.220	0.134
12-1734	0.026	0.066	0.924	4.350	3.887	1.148	2.956	4.965	2.383	-0.136	1.382	-3.284	0.217
	0.004	0.005	0.081	0.145	0.212	0.115	0.174	0.279	0.132	0.156	0.107	0.164	0.099
16-650	0.045	0.078	1.291	4.729	4.204	1.063	3.157	6.565	1.804	-0.690	0.657	-5.776	-1.733
	0.007	0.008	0.118	0.219	0.300	0.158	0.229	0.366	0.190	0.239	0.163	0.250	0.151
22-790	0.032	0.072	1.238	5.190	4.660	1.207	3.009	6.198	1.702	-0.905	0.355	-5.421	-1.262
	0.006	0.007	0.098	0.166	0.227	0.121	0.177	0.269	0.117	0.214	0.147	0.191	0.115
6-1553	-0.004	0.036	0.852	4.887	4.153	1.145	3.186	6.409	2.147	0.831	1.011	-3.903	-0.556
	0.030	0.004	0.061	0.099	0.141	0.071	0.102	0.155	0.068	0.116	0.081	0.115	0.071
6-1676	0.002	0.024	1.052	4.539	3.957	0.899	2.823	5.366	2.351	-0.178	1.373	-4.063	-0.516
	0.006	0.007	0.097	0.173	0.250	0.134	0.202	0.313	0.140	0.205	0.139	0.196	0.119
7-2322	0.068	0.105	1.285	5.402	4.171	1.209	3.131	6.699	1.575	-1.272	0.670	-5.516	-1.503
	0.009	0.010	0.154	0.271	0.374	0.194	0.282	0.438	0.226	0.321	0.217	0.315	0.192
9-2105	0.022	0.061	0.795	4.916	4.818	0.806	3.341	6.626	1.985	1.166	1.363	-4.403	-0.457
	0.014	0.017	0.238	0.397	0.508	0.265	0.367	0.517	0.212	0.486	0.337	0.446	0.264
10-112	-0.041	-0.012	0.711	3.471	2.967	0.697	2.223	4.170	2.869	2.888	2.449	-0.672	1.285
	0.006	0.008	0.119	0.224	0.319	0.170	0.253	0.413	0.217	0.216	0.152	0.236	0.143
1256-5723	-0.005	0.025	0.807	3.310	2.895	0.657	2.617	4.930	2.994	2.209	2.461	-1.340	0.969
	0.004	0.005	0.074	0.135	0.195	0.103	0.155	0.241	0.106	0.144	0.099	0.142	0.087
13-3813	0.038	0.086	1.072	4.962	4.768	0.886	2.871	6.047	1.941	-0.037	0.991	-4.845	-0.985
	0.006	0.007	0.099	0.169	0.238	0.131	0.194	0.300	0.133	0.201	0.138	0.196	0.119
16-1302	0.076	0.121	1.099	5.284	4.704	1.141	2.951	6.901	2.160	-0.832	0.677	-5.162	-1.177
	0.005	0.006	0.093	0.153	0.212	0.115	0.171	0.261	0.117	0.193	0.131	0.180	0.109
17-2134	-0.020	0.019	0.814	3.326	3.589	0.817	2.407	4.673	2.983	2.380	2.308	-0.858	1.355
	0.005	0.006	0.091	0.162	0.228	0.124	0.188	0.294	0.180	0.179	0.125	0.173	0.106
8-2119	-0.045	-0.005	0.823	3.345	2.892	0.592	2.357	4.183	3.381	2.620	2.599	-1.270	1.145
	0.007	0.009	0.134	0.254	0.356	0.188	0.276	0.451	0.235	0.247	0.171	0.266	0.161
3-601	0.026	0.071	0.872	4.556	3.681	0.900	2.944	5.805	—	0.648	1.557	-3.724	-0.451
	0.003	0.004	0.057	0.103	0.151	0.080	0.122	0.207	—	0.107	0.073	0.117	0.072
5-994	0.017	0.060	0.929	4.683	3.945	0.824	2.757	5.290	2.271	-0.050	1.105	-3.705	-0.255
	0.006	0.007	0.106	0.178	0.235	0.123	0.173	0.263	0.109	0.222	0.152	0.195	0.117
9-3079	0.019	0.114	1.186	5.680	4.302	0.943	3.408	6.469	1.758	-1.691	0.489	-6.803	-2.012
	0.008	0.008	0.123	0.217	0.307	0.161	0.229	0.369	0.197	0.251	0.167	0.261	0.156

Table A1. Lick/IDS line-strength indices within an aperture of $1 r_{\text{eff}}$ in our sample of galaxies. The wavelength coverage allowed us to measure 13 of the 25 indices. The second row for each galaxy lists the associated uncertainties in the respective indices.

1-2874	0.045	0.079	0.988	5.301	4.422	1.161	2.993	6.584	—	-1.013	0.491	-5.730	-1.201
	0.006	0.007	0.107	0.190	0.269	0.142	0.210	0.336	—	0.212	0.144	0.223	0.134
11-1278	0.107	0.149	1.081	5.481	5.221	1.050	3.117	7.778	2.108	-1.042	0.208	-6.090	-1.241
	0.006	0.007	0.101	0.166	0.224	0.121	0.179	0.267	0.119	0.220	0.148	0.195	0.118
11-1732	-0.019	0.005	0.523	3.159	2.856	0.344	2.617	4.986	2.890	2.422	2.277	-1.707	0.974
	0.003	0.004	0.064	0.116	0.170	0.093	0.136	0.217	0.105	0.115	0.078	0.124	0.076
14-1401	0.046	0.078	1.255	5.565	4.210	1.062	3.046	5.048	1.810	-1.587	0.747	-5.361	-1.381
	0.010	0.012	0.160	0.269	0.359	0.183	0.262	0.385	0.167	0.375	0.251	0.307	0.186
17-596	0.081	0.113	1.081	5.304	4.604	0.840	2.948	6.786	1.882	-1.621	0.540	-6.133	-1.621
	0.005	0.006	0.084	0.143	0.197	0.106	0.154	0.232	0.101	0.178	0.118	0.167	0.101
17-681	0.068	0.100	1.242	5.376	4.338	0.943	3.020	7.016	1.656	-1.141	0.582	-6.180	-1.838
	0.007	0.008	0.123	0.207	0.276	0.146	0.208	0.306	0.134	0.259	0.175	0.240	0.144
19-2242	0.033	0.068	0.998	5.042	3.929	0.945	2.973	5.565	2.036	-0.987	0.855	-4.997	-1.104
	0.003	0.004	0.059	0.107	0.156	0.084	0.123	0.195	0.093	0.120	0.080	0.126	0.076
19-2206	0.060	0.094	1.281	5.325	4.305	1.040	3.308	5.775	1.924	-1.329	0.574	-6.315	-1.760
	0.006	0.007	0.105	0.192	0.271	0.145	0.206	0.331	0.159	0.223	0.148	0.228	0.137
2-3070	0.019	0.046	1.298	5.279	4.229	0.910	3.327	4.357	1.542	-1.997	0.299	-5.280	-1.294
	0.008	0.010	0.136	0.242	0.333	0.175	0.254	0.395	0.181	0.305	0.207	0.281	0.170
2-3102	0.058	0.096	1.279	5.631	4.132	1.221	3.373	5.539	1.697	-2.000	0.993	-5.557	-1.380
	0.011	0.013	0.180	0.315	0.447	0.237	0.348	0.543	0.253	0.404	0.269	0.376	0.228

Table A1. Continue

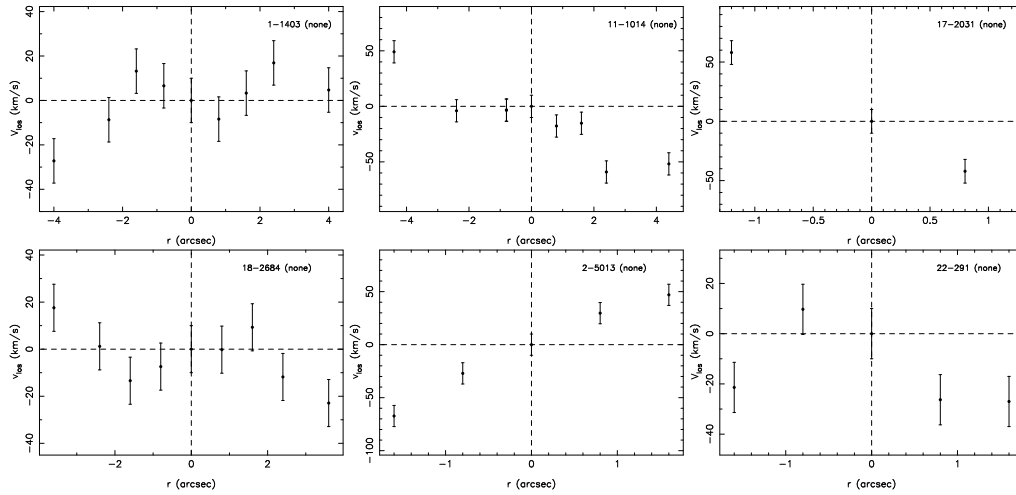


Figure B1. Rotation curves for undisturbed galaxies

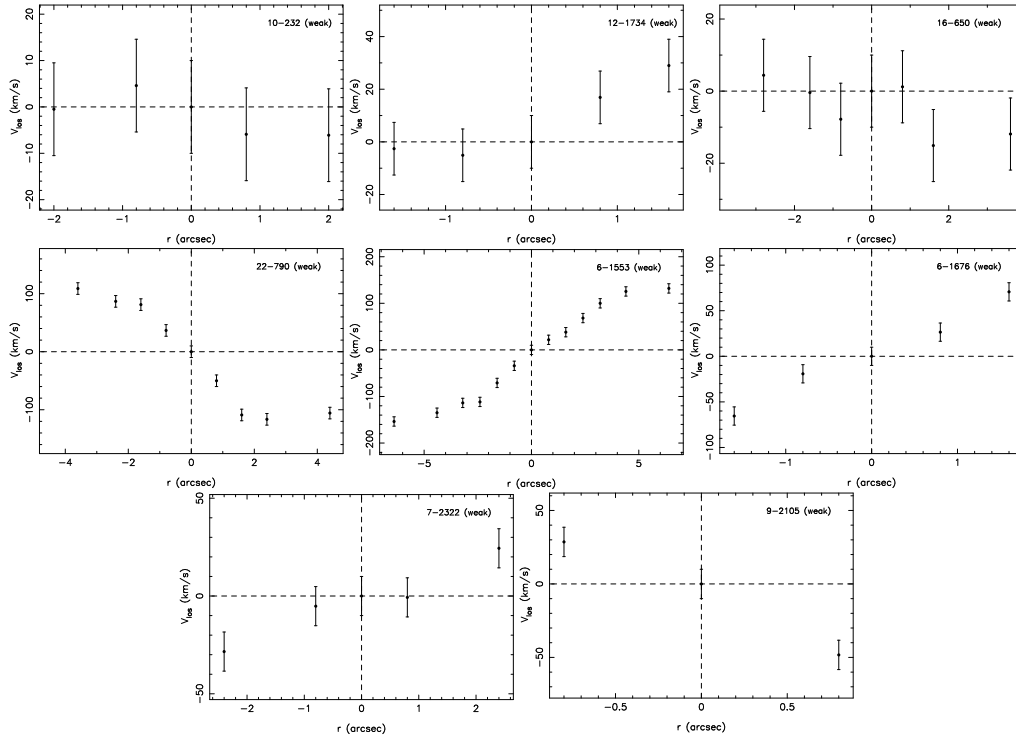


Figure B1. Rotation curve for galaxies showing weak morphological disturbances.

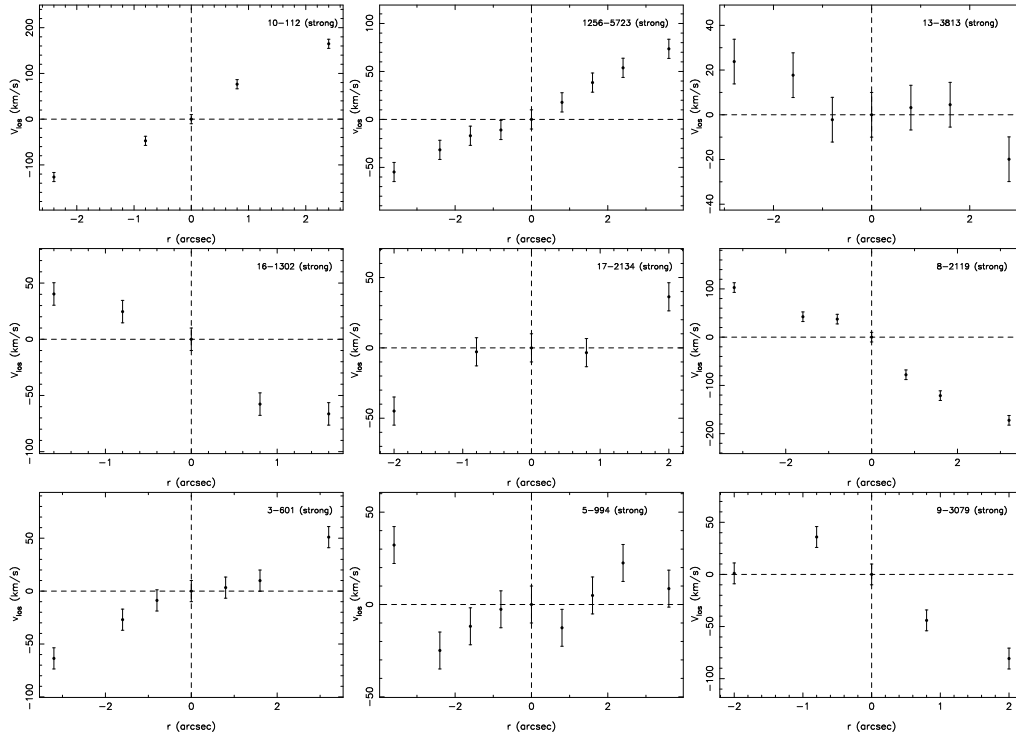


Figure B1. Rotation curves for galaxies showing strong morphological disturbances.

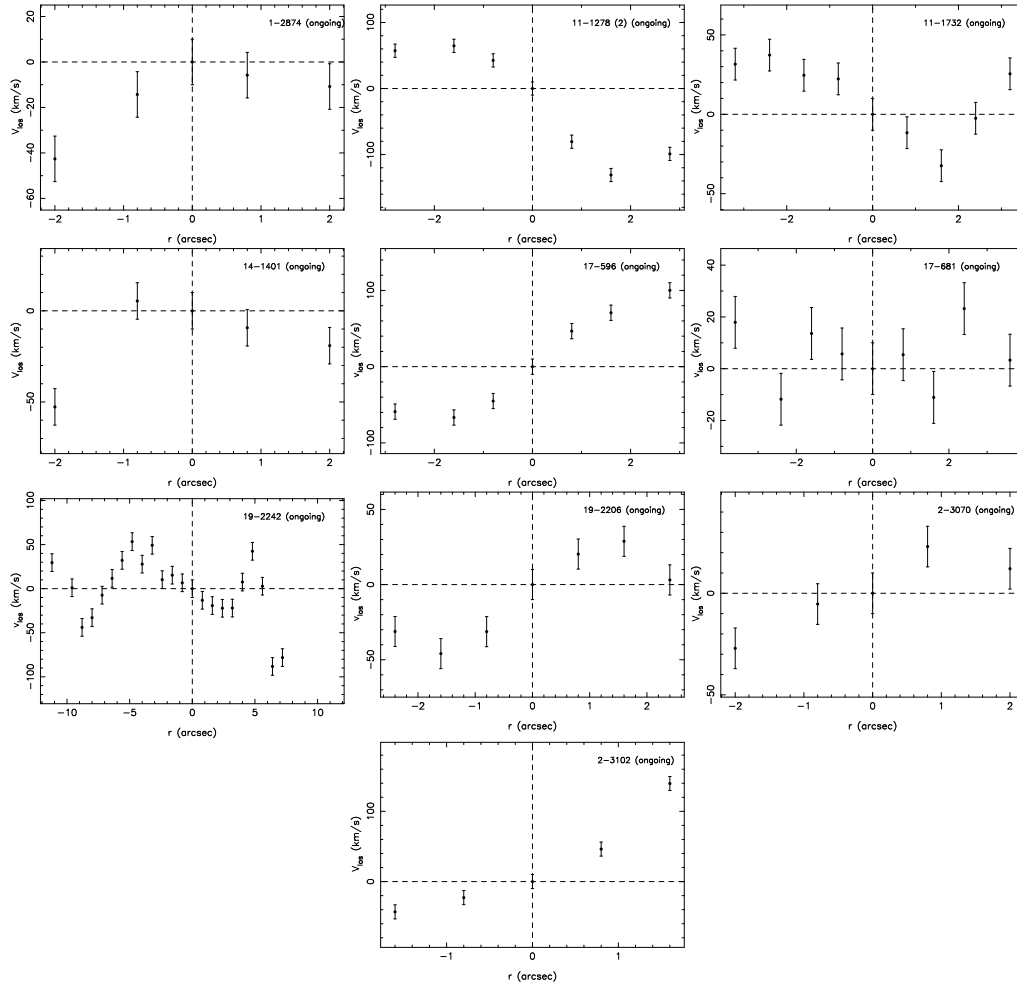


Figure B1. Rotation curves for galaxies in ongoing interactions.